Universality of nucleon-nucleon short-range correlations: The factorization property of the nuclear wave function, the relative and center-of-mass momentum distributions, and the nuclear contacts

M. Alvioli,[1,*] C. Ciofi degli Atti,[2,†] and H. Morita[3,‡]

[1] *CNR-IRPI, Istituto di Ricerca per la Protezione Idrogeologica, Via Madonna Alta 126, I-06128, Perugia, Italy*

[2] *Istituto Nazionale di Fisica Nucleare, Sezione di Perugia, c/o Department of Physics and Geology, University of Perugia, Via A. Pascoli, I-06123, Italy*

[3] *Sapporo Gakuin University, Bunkyo-dai 11, Ebetsu 069-8555, Hokkaido, Japan*

(Received 17 July 2016; published 11 October 2016)

Background: The two-nucleon momentum distributions of nucleons N_1 and N_2 in a nucleus A, $n_A^{N_1N_2}(\mathbf{k}_{\rm rel},\mathbf{K}_{\rm c.m.})$, is a relevant quantity that determines the probability of finding two nucleons with relative momentum $\mathbf{k}_{\rm rel}$ and center-of-mass (c.m.) momentum $\mathbf{K}_{\rm c.m.}$; at high values of the relative momentum and, at the same time, low values of the c.m. momentum, $n_A^{N_1N_2}(\mathbf{k}_{\rm rel},\mathbf{K}_{\rm c.m.})$ provides information on the short-range structure of nuclei.

Purpose: Our purpose is to calculate the momentum distributions of proton-neutron and proton-proton pairs in ^{3}He, ^{4}He, ^{12}C, ^{16}O, and ^{40}Ca, in correspondence to various values of $\mathbf{k}_{\rm rel}$ and $\mathbf{K}_{\rm c.m.}$.

Methods: The momentum distributions for $A > 4$ nuclei are calculated as a function of the relative, $k_{\rm rel}$, and center-of-mass, $K_{\rm c.m.}$, momenta and relative angle Θ, within a linked cluster many-body expansion approach, based upon realistic local two-nucleon interaction of the Argonne family and variational wave functions featuring central, tensor, and spin-isospin correlations.

Results: Independently of the mass number A, at values of the relative momentum $k_{\rm rel} \gtrsim 1.5$–2 fm^{-1} the momentum distributions exhibit the property of factorization, $n_A^{N_1N_2}(\mathbf{k}_{\rm rel},\mathbf{K}_{\rm c.m.}) \simeq n_{\rm rel}^{N_1N_2}(k_{\rm rel})n_{\rm c.m.}^{N_1N_2}(K_{\rm c.m.})$; in particular, for pn back-to-back pairs one has $n_A^{pn}(k_{\rm rel},K_{\rm c.m.}=0) \simeq C_A^{pn}n_D(k_{\rm rel})n_{\rm c.m.}^{pn}(K_{\rm c.m.}=0)$, where n_D is the deuteron momentum distribution, $n_{\rm c.m.}^{pn}(K_{\rm c.m.}=0)$ the c.m. motion momentum distribution of the pair, and C_A^{pn} the pn nuclear contact measuring the number of back-to-back pn pairs with deuteron-like momenta ($\mathbf{k}_p \simeq -\mathbf{k}_n,\mathbf{K}_{\rm c.m.}=0$).

Conclusions: The values of the pn nuclear contact are extracted from the general properties of the two-nucleon momentum distributions corresponding to $K_{\rm c.m.}=0$. The $K_{\rm c.m.}$-integrated pn momentum distributions exhibit the property $n_A^{pn}(k_{\rm rel}) \simeq C_A^{pn}n_D(k_{\rm rel})$ but only at very high values of $k_{\rm rel}$, $\gtrsim$3.5–4 fm^{-1}. The theoretical ratio of the pp/pn momentum distributions of ^{4}He and ^{12}C and the calculated c.m. motion momentum distributions are in agreement with recent experimental data.

DOI: 10.1103/PhysRevC.94.044309

I. AIM AND INTRODUCTION

The investigation of short-range correlations (SRCs) in nuclei is ultimately aimed at unveiling the details of in-medium short-range nucleon-nucleon (NN) dynamics, a relevant physics issue that cannot be answered by scattering experiments of two free nucleons (see recent review papers on the subject [1–5]). A reliable way to gather information on SRCs would be to detect significant deviations of proper experimental data (e.g., electrodisintegration processes off nuclei) from theoretical predictions based upon *ab initio* solutions of the nuclear many-body problem, obtained from various NN interactions differing in the short-range part. In practice, such an approach faces several problems because it implies the exact calculation of the ground- and continuum-state wave functions of the target nucleus under investigation; concerning the former, relevant progress has recently been made to obtain *ab initio* solutions of the nonrelativistic Schrödinger equation, but unfortunately, the treatment of the continuum spectrum of the target nucleus is still model dependent, with the only exception of those processes involving the two- and three-nucleon systems. For complex nuclei approximations are unavoidable, with the simplest one being the plane-wave impulse approximation (PWIA), which leads, in the case of, e.g., a process $A(e,e'N)X$, to a factorized cross section depending upon the elementary electron-nucleon cross section and the one-nucleon spectral function $P_A(E,k)$, which describes the momentum ($k \equiv |\mathbf{k}|$) and removal energy (E) distributions of a nucleon in nucleus A [in a process $A(e,e'N_1N_2)X$ the factorized cross section will depend upon the two-nucleon spectral function, etc.]. Even if the PWIA requires corrections due to the final-state interaction (FSI) and possible effects from non-nucleonic degrees of freedom, the detection of high-momentum and high-removal-energy effects may represent evidence of ground-state SRCs. It is for this reason that during the last few years, calculation of the nuclear momentum distributions and spectral function has attracted increasing interest. The one-nucleon, $n_A(k_1)$, and two-nucleon, $n_A(\mathbf{k}_1,\mathbf{k}_2)$, momentum distributions of few-nucleon systems ($A \leqslant 4$) have been obtained *ab initio* [6–10] within different theoretical approaches and using realistic NN interactions, whereas for $A \leqslant 12$ exact variational Monte Carlo (VMC) calculations have recently been performed [11].

*massimiliano.alvioli@irpi.cnr.it

†ciofi@pg.infn.it

‡hiko@webmail.sgu.ac.jp

For nuclei with $A > 12$, VMC calculations of the momentum distribution are not yet feasible, therefore, also in light of future experimental developments, alternative approaches, even if of a lower quality than VMC ones, but still maintaining a realistic link to the underlying NN interactions, should be pursued. A serious candidate in this respect would be an advanced linked cluster expansion approach with correlated wave functions, including a large class of Yvon-Mayer diagrams [12–14], for they have been shown to produce realistic results of one-nucleon momentum distributions [15–17] in reasonable agreement with the more advanced VMC calculations. All of these calculations, though being performed within different many-body approaches, produce similar results demonstrating a universal (A-independent) character of in-medium NN short-range dynamics, in that the mean-field approach breaks down when the relative distance $r \equiv |\boldsymbol{r}_1 - \boldsymbol{r}_2|$ between two generic nucleons "1" and "2" is of the order of $r \lesssim 1.3$–1.5 fm, with the two-nucleon density distribution exhibiting the so-called *correlation hole*, which, apart from trivial normalization factors, turns out to be independent of the mass A of the nucleus and similar to the deuteron one. SRCs give rise to high-momentum components that are lacking in a mean-field approach and turned out to depend upon the relative orbital momentum (L) and the total spin (S) and isospin (T) of the NN pair, as well as upon the value of the pair center-of-mass (c.m.) momentum. SRCs give rise to peculiar configurations of the nuclear wave function in momentum space, e.g., ones where a high-momentum nucleon is mostly balanced by another nucleon with similar and opposite value of the momentum [the *back-to-back* (BB) configuration] and not by the $A-1$ nucleon, as in the case of a mean-field configuration [18]. Thus, within a PWIA picture, if a correlated nucleon, with momentum $\boldsymbol{k}_1$, acquiring a momentum $\boldsymbol{q}$ from an external probe, leaves the nucleus without any FSI and is detected with momentum $\boldsymbol{p} = \boldsymbol{k}_1 + \boldsymbol{q}$, the partner nucleon should be emitted with momentum $\boldsymbol{k}_2 \simeq \boldsymbol{p}_m = -\boldsymbol{k}_1$, where the measurable momentum $\boldsymbol{p}_m$ is the *missing momentum* $\boldsymbol{p}_m = \boldsymbol{q} - \boldsymbol{p}$. Such a basic picture of BB short-range correlated (SRCd) nucleons has recently been improved to a large extent by taking into account the FSI of the struck nucleon by advanced methods (see, e.g., Refs. [19–22]) and by considering the effects due to the c.m. motion of the pair, which makes $\boldsymbol{k}_2 \neq -\boldsymbol{k}_1$, and the effects due to the (ST) dependence. The underlying dynamics of SRCs has been theoretically explained by advanced many-body theories, e.g., by the Brueckner-Bethe-Goldstone approach for nuclear matter [23] and by exact few-nucleon approaches in the case of ^{3}He and ^{4}He [24], with both approaches demonstrating that two-nucleon correlations arise from a general property of the many-body wave function, namely, its factorized form in those configurations where a pair of nucleons has, at the same time, a large value of the two-nucleon relative momentum $\boldsymbol{k}_{\rm rel}$ and a low value of the c.m. momentum $\boldsymbol{K}_{\rm c.m.}$, in agreement with the phenomenological assumption in Ref. [25]. The presence of SRCs in nuclei and their basic back-to-back nature have eventually been experimentally demonstrated [26–31], but detailed theoretical and experimental information through the periodic Table of the Elements on their isospin, angular, and c.m. momentum dependencies remains to be obtained. To contribute to this challenge in the present paper the results of calculations of the following quantities, pertaining to nuclei ^{3}He, ^{4}He, ^{12}C, ^{16}O, and ^{40}Ca, are presented: (i) the two-nucleon momentum distribution $n_A^{N_1N_2}$ of the proton-neutron (pn) and proton-proton (pp) pairs in correspondence with different values of the c.m. and the the relative momenta of the pair and the angle Θ between them; (ii) the number of short-range correlated pp and pn pairs represented by the integral of the various types of momentum distributions in a finite momentum range; and (iii) the ratio of the pn-to-pp correlated pairs *vs* the relative momentum $k_{\rm rel}$. Particular attention is devoted to the comparison of the two-nucleon momentum distributions of complex nuclei with the deuteron momentum distribution, in order to clarify whether and to what extent the short-range dynamics of a free bound pn system will differ from the short-range dynamics of a pn pair embedded in the medium. Calculations have been performed with realistic nuclear wave functions [15,32–34] obtained from the solution of the Schrödinger equation with realistic NN interactions, namely, the AV18 [35] and AV8′ [36] interactions. Various properties of the momentum distributions and various relations between them are illustrated, which further demonstrates the relevant property of the nuclear wave function in the correlation region, i.e., its factorized form. The quantity (the *nuclear contact*) measuring the number of deuteron-like pairs in nuclei is extracted from the general properties of the pn momentum distributions. The structure of the paper is as follows: in Sec. II the general definitions of the two-nucleon momentum distributions and their SRCd parts are given; the calculation of the momentum distributions and the universal, A-independent behavior of their SRCd parts are presented in Sec. III; the general validity of the factorization property in the SRC region is proved in Sec. IV; the numbers of SRCd pn and pp pairs in various regions of $k_{\rm rel}$ and $K_{\rm c.m.}$ are given in Sec. V; a comparison between the available experimental data and the theoretical predictions is presented in Sec. VI; and a summary and conclusions are given in Sec. VII.

II. GENERAL DEFINITIONS

In this paper the numbers of protons and neutrons in nucleus A are denoted Z and N, respectively, with $A = Z + N$. The two-body momentum distribution of a pair of nucleons N_1N_2, summed over spin (S) and isospin (T) states, is given by

$$n_A^{N_1N_2}(\boldsymbol{k}_1,\boldsymbol{k}_2) = \frac{1}{(2\pi)^6}\int d\boldsymbol{r}_1\, d\boldsymbol{r}_2\, d\boldsymbol{r}'_1\, d\boldsymbol{r}'_2\, e^{i\,\boldsymbol{k}_1\cdot(\boldsymbol{r}_1-\boldsymbol{r}'_1)} \times e^{i\,\boldsymbol{k}_2\cdot(\boldsymbol{r}_2-\boldsymbol{r}'_2)}\,\rho^{(2)}_{N_1N_2}(\boldsymbol{r}_1,\boldsymbol{r}_2;\boldsymbol{r}'_1,\boldsymbol{r}'_2), \quad (1)$$

where

$$\rho^{(2)}_{N_1N_2}(\boldsymbol{r}_1,\boldsymbol{r}_2;\boldsymbol{r}'_1,\boldsymbol{r}'_2) = \int \psi_o^*(\boldsymbol{r}_1,\boldsymbol{r}_2,\boldsymbol{r}_3\ldots,\boldsymbol{r}_A)\,\psi_o \times(\boldsymbol{r}'_1,\boldsymbol{r}'_2,\boldsymbol{r}_3,\ldots,\boldsymbol{r}_A)\,\delta\left(\sum_{i=1}^{A}\boldsymbol{r}_i\right)\prod_{i=3}^{A} d\boldsymbol{r}_i \quad (2)$$

is the two-body nondiagonal density matrix of nucleus A. The normalization of the proton, neutron, and total distributions, unless differently stated, is[1]

$$\int n_A^{N_1N_2}(\boldsymbol{k}_1,\boldsymbol{k}_2)d\boldsymbol{k}_1\, d\boldsymbol{k}_2 = \int \rho^{(2)}_{N_1N_2}(\boldsymbol{r}_1,\boldsymbol{r}_2)d\boldsymbol{r}_1\, d\boldsymbol{r}_2$$
$$= \frac{Z(Z-1)}{2}\bigg|_{N_1=N_2=p}$$
$$= \frac{N(N-1)}{2}\bigg|_{N_1=N_2=n}$$
$$= ZN\,|_{N_1=p,N_2=n}, \qquad (3)$$

with

$$\sum_{N_1N_2}\int n_A^{N_1N_2}(\boldsymbol{k}_1,\boldsymbol{k}_2)d\boldsymbol{k}_1\, d\boldsymbol{k}_2 = \sum_{N_1N_2}\int \rho^{(2)}_{N_1N_2}(\boldsymbol{r}_1,\boldsymbol{r}_2)d\boldsymbol{r}_1\, d\boldsymbol{r}_2$$
$$= \frac{A(A-1)}{2}. \qquad (4)$$

By introducing the relative and c.m. two-nucleon coordinates and momenta [$\boldsymbol{r} = \boldsymbol{r}_1 - \boldsymbol{r}_2$, $\boldsymbol{k}_{\rm rel} = (\boldsymbol{k}_1 - \boldsymbol{k}_2)/2$; $\boldsymbol{R} = (\boldsymbol{r}_1 + \boldsymbol{r}_2)/2$, $\boldsymbol{K}_{\rm c.m.} = \boldsymbol{k}_1 + \boldsymbol{k}_2$], the two-nucleon momentum distribution can be rewritten as [10]

$$n_A^{N_1N_2}(\boldsymbol{k}_{\rm rel},\boldsymbol{K}_{\rm c.m.}) = n_A^{N_1N_2}(k_{\rm rel},K_{\rm c.m.},\Theta)$$
$$= \frac{1}{(2\pi)^6}\int d\boldsymbol{r}\, d\boldsymbol{R}\, d\boldsymbol{r}'\, d\boldsymbol{R}'\, e^{i\,\boldsymbol{K}_{\rm c.m.}\cdot(\boldsymbol{R}-\boldsymbol{R}')}$$
$$e^{i\,\boldsymbol{k}_{\rm rel}\cdot(\boldsymbol{r}-\boldsymbol{r}')}\,\rho^{(2)}_{N_1N_2}(\boldsymbol{r},\boldsymbol{R};\boldsymbol{r}',\boldsymbol{R}'), \qquad (5)$$

where $|\boldsymbol{k}_{\rm rel}| \equiv k_{\rm rel}$, $|\boldsymbol{K}_{\rm c.m.}| \equiv K_{\rm c.m.}$, and Θ is the angle between $\boldsymbol{k}_{\rm rel}$ and $\boldsymbol{K}_{\rm c.m.}$. Of particular interest is the quantity

$$n_A^{pn}(k_{\rm rel},K_{\rm c.m.}=0) = \frac{1}{(2\pi)^3}\int d\boldsymbol{r}\, d\boldsymbol{r}'\, e^{i\,\boldsymbol{k}_{\rm rel}\cdot(\boldsymbol{r}-\boldsymbol{r}')}\,\rho^{(2)}_{pn}(\boldsymbol{r},\boldsymbol{r}'), \qquad (6)$$

describing the spin and isospin summed relative momentum distributions of BB pairs, $\rho^{(2)}_{pn}(\boldsymbol{r},\boldsymbol{r}')$ being the c.m.-integrated nondiagonal two-body density matrix. Relevant quantities are also the $K_{\rm c.m.}$- and $k_{\rm rel}$-integrated momentum distributions, namely,

$$n_A^{N_1N_2}(k_{\rm rel}) = \int n_A^{N_1N_2}(\boldsymbol{k}_{\rm rel},\boldsymbol{K}_{\rm c.m.})\, d\,\boldsymbol{K}_{\rm c.m.} \qquad (7)$$

and

$$n_A^{N_1N_2}(K_{\rm c.m.}) = \int n_A^{N_1N_2}(\boldsymbol{k}_{\rm rel},\boldsymbol{K}_{\rm c.m.})d\,\boldsymbol{k}_{\rm rel}. \qquad (8)$$

Equations (6)–(8) have been calculated in Refs. [7–11] for ^{3}He and ^{4}He, using *ab initio* wave functions and in Ref. [11] for ^{6}He, ^{8}He, ^{6}Li, ^{7}Li, ^{8}Li, ^{9}Li, ^{8}Be, ^{9}Be, ^{10}Be, ^{10}B, and, preliminarily, ^{12}C, within the VMC approach. In this paper we describe new results for various momentum distributions in ^{3}He, ^{4}He, ^{12}C, ^{16}O, and ^{40}Ca obtained, in the case of few-nucleon systems ($A = 3,4$), with *ab initio* wave functions and, in the case of nuclei with $A > 4$, within a linked-cluster expansion up to the order of four-body cluster contributions [15]. Whenever possible the results of our calculations of the momentum distributions are compared with the results of the VMC approach in Ref. [11].[2]

III. RESULTS OF CALCULATIONS AND UNIVERSAL PROPERTIES OF THE CORRELATED TWO-NUCLEON MOMENTUM DISTRIBUTIONS

A. The two-nucleon momentum distribution in ^{3}He and isoscalar nuclei

In Figs. 1–6 we show (i) the *pn* and *pp* momentum distributions in ^{3}He, ^{4}He, ^{12}C, ^{16}O, and ^{40}Ca nuclei, in particular, the full two-nucleon momentum distribution $n_A^{N_1N_2}(k_{\rm rel},K_{\rm c.m.},\Theta)$ [Eq. (5)]; (ii) the back-to-back momentum distributions [Eq. (6)]; (iii) the relative momentum distributions, Eq. (7); and (iv) the c.m. momentum distribution [Eq. (8). The results presented in these figures have been obtained using microscopic wave functions corresponding to the AV18 interaction [35] for ^{2}H and ^{3}He [32,33] and the AV8′ interaction [36] for ^{4}He [34] and complex nuclei [15]. In order to compare our results with the VMC results in Ref. [11], whose wave functions are calculated with the 2N AV18 + 3N UX interaction, we present in Fig. 7 the one-nucleon momentum distributions for $A = 4$ and $A = 12$ obtained by the two approaches, because both quantities will be used in what follows. Concerning our parameter-free results, let us first stress that they are in a general reasonable agreement with the results of the VMC calculation [11], although in some regions of momenta (e.g. at $2.5 \lesssim k_{\rm rel} \lesssim 3.5$ fm^{-1}) they can differ appreciably, within 10%–20%, particularly in the case of the *pp* relative momentum distribution of ^{4}He and ^{12}C; the possible origin of this disagreement, which does not appear to be due to the effects of the 3N force missing in our calculation [37], is under investigation. The obtained momentum distributions of both few-nucleon systems and complex nuclei exhibit several universal features that can be summarized as follows:

(1) As first pointed out in Ref. [9] in the case of few-nucleon systems, when $K_{\rm c.m.} = 0$, the *pn* and *pp* momentum distributions do not appreciably differ at small values of $k_{\rm rel}$, with their ratio being closer to the ratio of the number of *pn* to the number of *pp* pairs, whereas in the region $1.0 \lesssim k_{\rm rel} \lesssim 4.0$ fm^{-1} the dominant role of tensor correlations makes the *pn* distribution much larger than the *pp* distribution, with the node exhibited by the latter filled up by the *D* wave in the *pn* two-body density.

(2) Figures 1(a), 1(b), 2(a), and 2(b) show that the momentum distribution $n_A^{\rm NN}(k_{\rm rel},K_{\rm c.m.},\Theta)$, plotted vs $k_{\rm rel}$, decreases, at low and high values of $k_{\rm rel}$, with increasing values of $K_{\rm c.m.}$, whereas at intermediate values of $k_{\rm rel}$

[1]Note that in Ref. [10] the two-nucleon momentum distributions were normalized to 1 in the case of ^{4}He, whereas in the case of ^{3}He they were normalized to the number of *pn* and *pp* pairs, i.e., 2 and 1, respectively.

[2]In this paper we mainly discuss the spin-isospin summed momentum distributions of isoscalar nuclei, whereas the spin-isospin-dependent momentum distribution of nonisoscalar nuclei will be the object of future investigations.

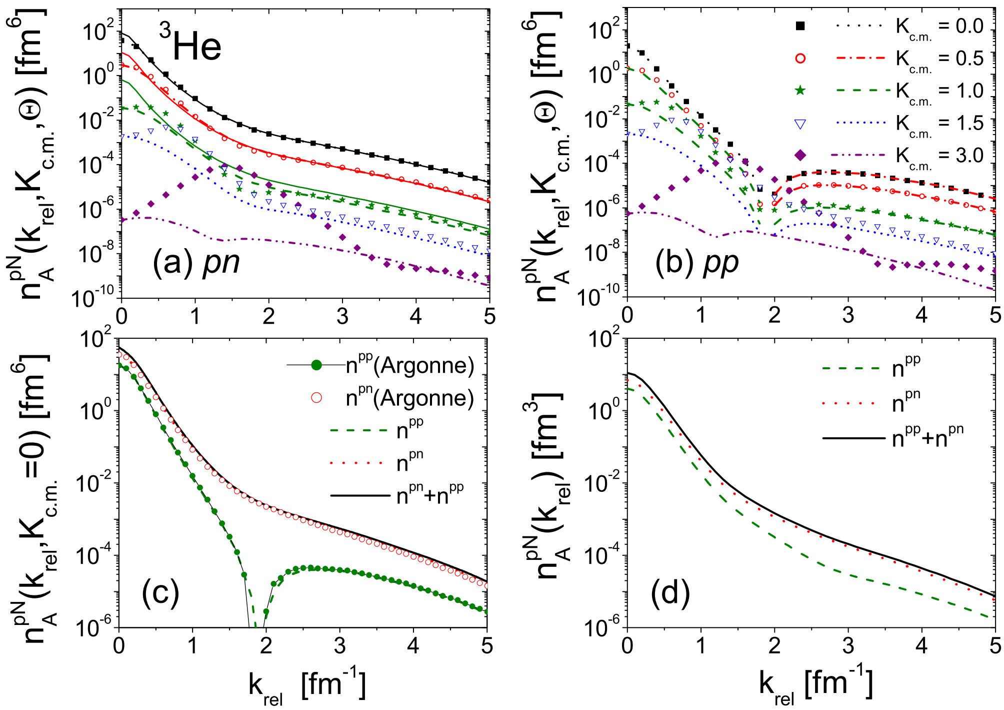

FIG. 1. (a) Two-nucleon momentum distributions of pn pairs in ^{3}He vs the relative momentum $k_{\rm rel}$ for fixed values of the c.m. momentum $K_{\rm c.m.}$ (in fm^{-1}) and two values of the angle Θ between $\mathbf{k}_{\rm rel}$ and $\mathbf{K}_{\rm c.m.}$, namely, $\Theta = 90^\circ$ (broken curves) and $\Theta = 0^\circ$ (symbols). In this figure, and only in it, solid curves represent Eq. (10) with $C_3^{pn} = 2.0$. ^{3}He wave function from Refs. [32,33] and AV18 interaction [35]. (b) Same as (a), but for pp pairs. (c) The pn and pp distributions corresponding to $K_{\rm c.m.} = 0$ in (a) and (b) and their sum. (d) Relative two-body momentum distributions $n_A^{N_1N_2}(k_{\rm rel}) = \int n_A^{N_1N_2}(\boldsymbol{k}_{\rm rel}, \boldsymbol{K}_{\rm c.m.})\, d\,\boldsymbol{K}_{\rm c.m.}$. In (c) open and filled circles represent the results from Argonne [11]. In this and the following figures, unless differently stated, pn and pp distributions are normalized to ZN and $Z(Z-1)/2$, respectively.

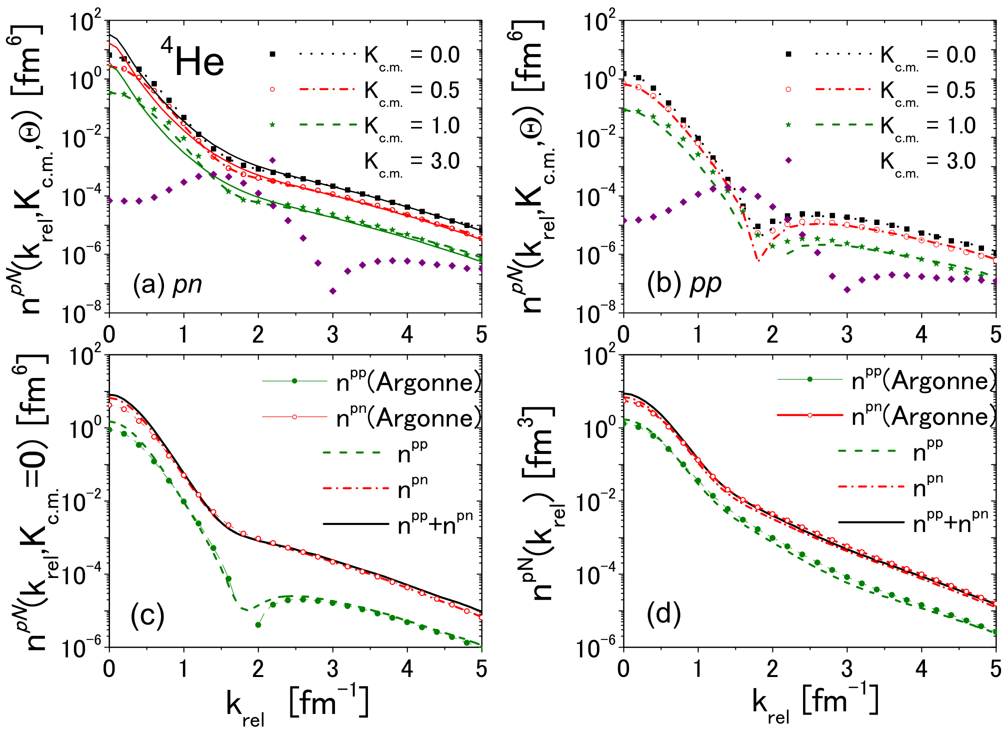

FIG. 2. Same as Fig. 1, but for ^{4}He with $C_4^{pn} = 4.0$ in (a). ^{4}He wave function from Ref. [34] and AV8$'$ interaction [36]. In (c) and (d) open and filled circles denote the results from Argonne [11].

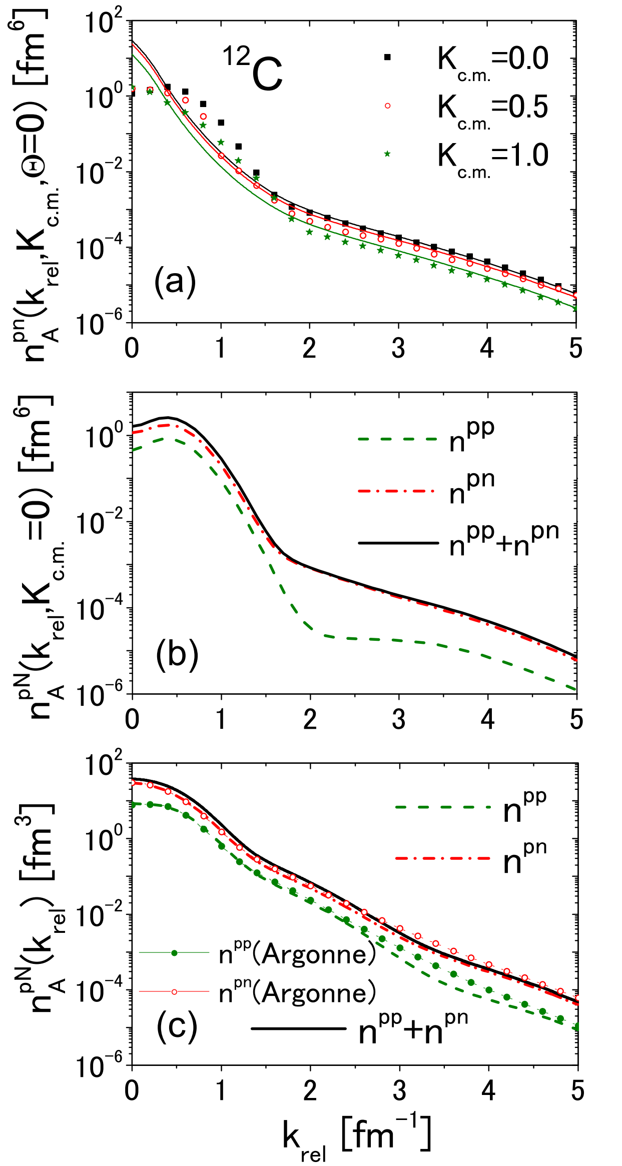

FIG. 3. Same as Fig. 1, but for ^{12}C with $C_{12}^{pn} = 20.0$ in (a). ^{12}C wave function from Ref. [15] and AV8′ interaction [36]. Note that here, as well as in Figs. 4 and 5, symbols in (a) correspond to $\Theta = 0$. In (c) open and filled circles represent the results from Argonne [11].

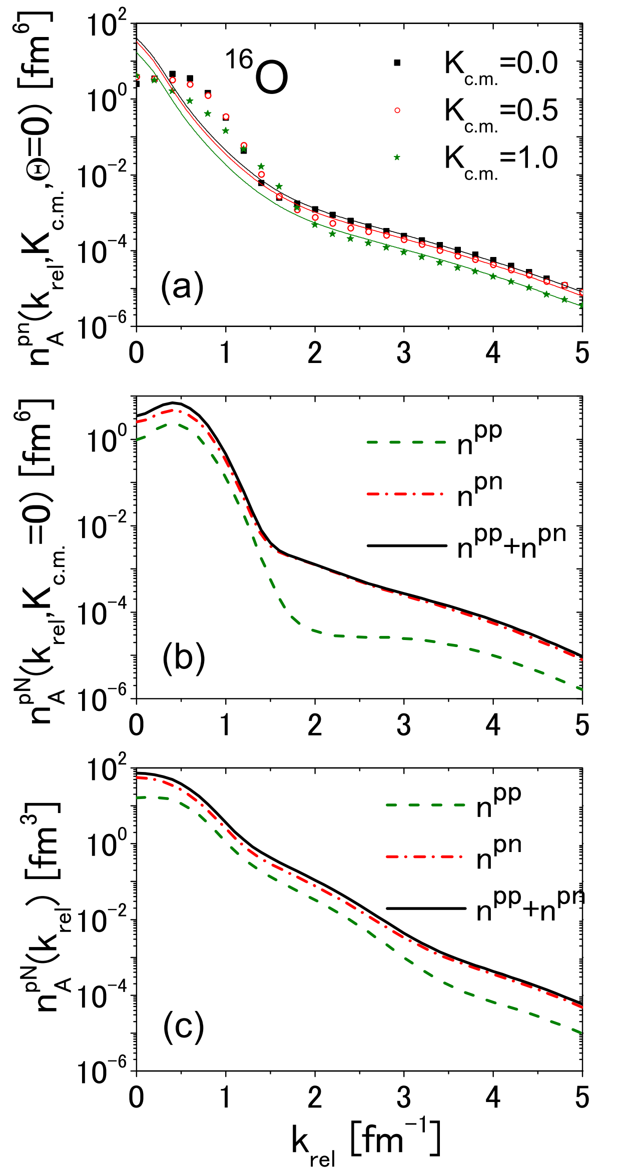

FIG. 4. Same as Fig. 1, but for ^{16}O with $C_{16}^{pn} = 24.0$ in (a). ^{16}O wave function from Ref. [15] and AV8′ interaction [36].

it increases with increasing values of $K_{\rm c.m.}$. This effect is particularly relevant for the *pp* case, where the dip occurring in the $K_{\rm c.m.} = 0$ distribution is totally washed out by the large $K_{\rm c.m.}$ components, resulting in a $K_{\rm c.m.}$-integrated distribution totally different from the one corresponding to $K_{\rm c.m.} = 0$ (cf.). This effect seems to hold in the case of complex nuclei as well, as illustrated by the differences exhibited in Figs. (b) and (c) for $A = 12$, 16, and 40 (Figs. 3, 4, and 5).

(3) Starting from a $K_{\rm c.m.}$-dependent value of the relative momentum $k_{\rm rel}$, denoted $k_{\rm rel}^-(K_{\rm c.m.})$, the *pn* two-nucleon momentum distributions become, to a large extent, Θ independent, with the value of $k_{\rm rel}^-(K_{\rm c.m.})$ increasing with $K_{\rm c.m.}$, according to the relation

$$k_{\rm rel}^-(K_{\rm c.m.}) = a_1 + f(K_{\rm c.m.}) \equiv k_{\rm rel}^-, \tag{9}$$

which can be defined with $a_1 \simeq 1.5$ fm^{-1} (cf. Figs. 1–5) and $f(K_{\rm c.m.}) = K_{\rm c.m.}$; Θ independence, first stressed in Ref. [17] and verified over a wide range of angles, implies that for $k_{\rm rel} > k_{\rm rel}^-$ the two-nucleon momentum distribution factorizes, i.e., $n_A^{N_1N_2}(k_{\rm rel},K_{\rm c.m.},\Theta) \propto n_{\rm rel}^{N_1N_2}(k_{\rm rel}) n_{\rm c.m.}^{N_1N_2}(K_{\rm c.m.})$. In the region of factorization, defined by $k_{\rm rel} \gtrsim k_{\rm rel}^-$ and $K_{\rm c.m.} \lesssim 1$ fm^{-1}, the momentum distribution for *pn* pairs can be approximated as follows:

$$n_A^{pn({\rm fact})}(k_{\rm rel},K_{\rm c.m.}) \simeq \frac{n_A^{pn}(k_{\rm rel},K_{\rm c.m.}=0)}{n_{\rm c.m.}^{pn}(K_{\rm c.m.}=0)}\, n_{\rm c.m.}^{pn}(K_{\rm c.m.}) \simeq C_A^{pn} n_D(k_{\rm rel}) n_{\rm c.m.}^{pn}(K_{\rm c.m.}). \tag{10}$$

Here $n_D(k_{\rm rel})$ is the deuteron momentum distribution, $n_{\rm c.m.}^{pn}(K_{\rm c.m.})$ the c.m. momentum distribution of the

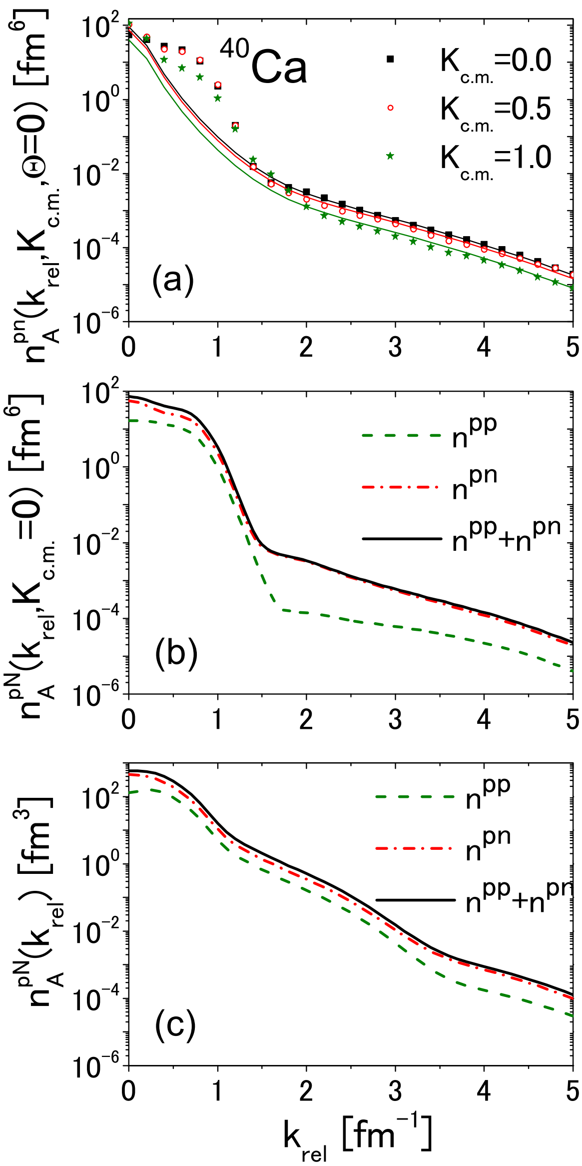

FIG. 5. Same as Fig. 1, but for ^{40}Ca with $C_{40}^{np} = 60.0$ in (a). ^{40}Ca wave function from Ref. [15] and AV8′ interaction [36].

correlated pair in the region of factorization, and C_A^{pn} an A-dependent constant, whose value and physical meaning are discussed in the next subsection. As for the pp momentum distribution, it appears that it also factorizes, but starting at a value of the relative momentum higher than $k_{\rm rel}(K_{\rm c.m.})^{-}$; one has

$$n_A^{pp({\rm fact})}(k_{\rm rel},K_{\rm c.m.}) \simeq \frac{n_A^{pp}(k_{\rm rel},K_{\rm c.m.}=0)}{n_{\rm c.m.}^{pp}(K_{\rm c.m.}=0)}\, n_{\rm c.m.}^{pp}(K_{\rm c.m.}) \simeq C_A^{pp} n_{\rm rel}^{pp}(k_{\rm rel}) n_{\rm c.m.}^{pp}(K_{\rm c.m.}). \qquad (11)$$

where, unlike the pn case, the momentum distribution $n_{\rm rel}^{pp}(k_{\rm rel})$ is, at the moment, not defined in terms of a pp system. Equations (10) and (11) describe a property exhibited in Figs. 1 and 2 (and common to any value of A), namely, that at high values of $k_{\rm rel} > k_{\rm rel}^{-}(K_{\rm c.m.})$

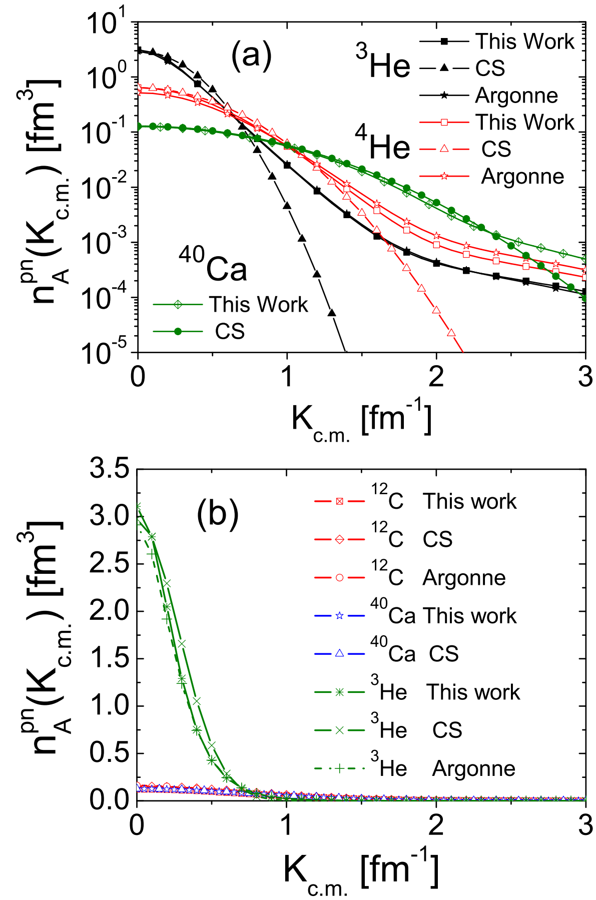

FIG. 6. (a) The center-of-mass (c.m.) momentum distribution $n_A^{pn}(K_{\rm c.m.}) = \int n_A^{pn}(\boldsymbol{k}_{\rm rel},\boldsymbol{K}_{\rm c.m.})\, d^3\boldsymbol{k}_{\rm rel}$ [Eq. (8)] in ^{3}He, ^{4}He, ^{12}C, and ^{40}Ca, normalized to 1, obtained in the present paper (this work), in Ref. [25] (CS), and in Ref. [11] (Argonne). Note that a Gaussian distribution related to the average value of the shell-model kinetic energy [25] agrees very well with the many-body realistic distribution up to $K_{\rm c.m.} \simeq 1$ fm^{-1} except in the case of ^{3}H, for which a shell-model description has no meaning. (b) The c.m. momentum distributions of ^{3}He, ^{12}C, and ^{40}Ca on a linear scale.

the pN momentum distributions differ only by their magnitudes, which are governed by $n_{\rm c.m.}^{pN}$.[3]

(4) At high values of the relative and c.m. momenta, more than two particles can be locally correlated, producing a strong dependence upon the angle Θ and, correspondingly, the violation of factorization, as shown in Fig. 1 in the case of $K_{\rm c.m.} = 3$ fm^{-1}; moreover, it can be seen [cf. Figs. 1(b) and 2(b)] that the behavior of n_A^{pp} in the region around $k_{\rm rel} \simeq 2$ fm^{-1} is strongly affected by the high $K_{\rm c.m.}$ momentum components.
(5) In Ref. [25] the low-momentum part ($K_{\rm c.m.} \lesssim 1.0$ fm^{-1}) of the c.m. momentum distribution has

[3]Note that $n_A^{N_1N_2}(K_{\rm c.m.})$ [Eq. (8)] includes all c.m. momentum components, whereas $n_{\rm c.m.}^{N_1N_2}(K_{\rm c.m.})$ has to describe only the low-momentum part ($K_{\rm c.m.} \lesssim 1$–1.5 fm^{-1}) of the c.m. motion.

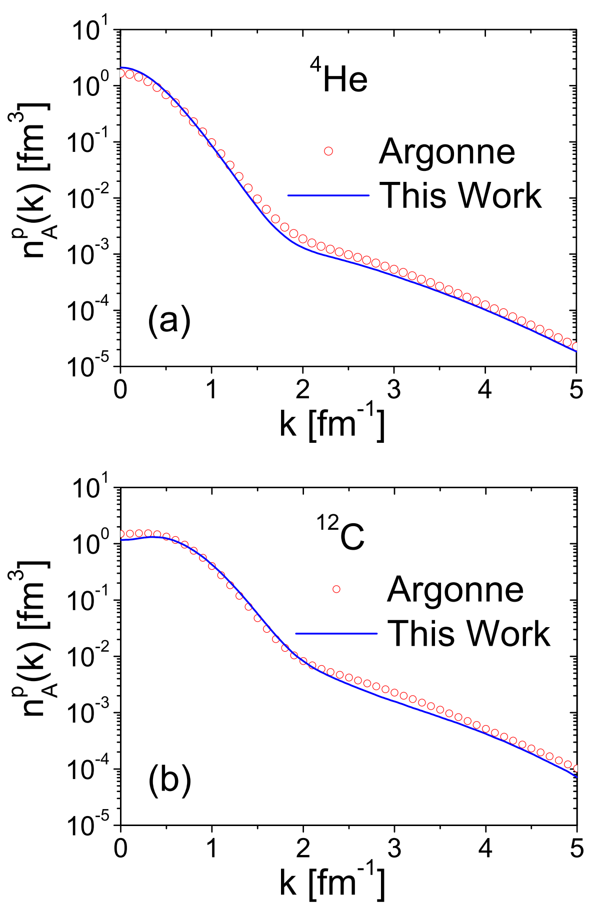

FIG. 7. Comparison of the one-nucleon momentum distributions of ^{4}He and ^{12}C calculated in Ref. [17] (solid line) and in Ref. [11] (open circles), respectively. Normalization to the number of protons Z.

been described by a Gaussian function normalized to 1, namely, $n^A_{\mathrm{c.m.}}(K_{\mathrm{c.m.}}) = (\alpha_A/\pi)^{3/2}\exp(-\alpha_A\, K^2_{\mathrm{c.m.}})$, with the values of α_A obtained from the average value of the shell model kinetic energy $\langle T\rangle_{\mathrm{SM}}$, as $\alpha_A = \frac{3(A-1)}{4m_N(A-2)\langle T\rangle_{\mathrm{SM}}}$. It can be seen from Fig. 6 that, apart from the case of ^{3}He, for which a shell-model description is meaningless, the Gaussian model in Ref. [25] nicely approximates the many-body result in the region of $K_{\mathrm{c.m.}} \lesssim 1$ fm^{-1}. The values of α_A for ^{4}He and ^{12}C obtained in Ref. [25] also agree with the experimental data [27,28,30], discussed in Sec. V.

B. The meaning and the numerical values of the quantity C_A^{pn}

In what follows we discuss in detail the behavior of the pn momentum distributions in the correlation region, in particular, the meaning and the numerical value of the constant C_A^{pn} appearing in Eq. (10). This is because we would like to compare the short-range behavior of a bound pn pair, i.e., the deuteron, with the behavior of a pn pair in the nuclear medium. The factorized form [Eq. (10)] describes 2N SRCd configurations when the relative momentum of the pair is much higher than the c.m. momentum. Since for isoscalar

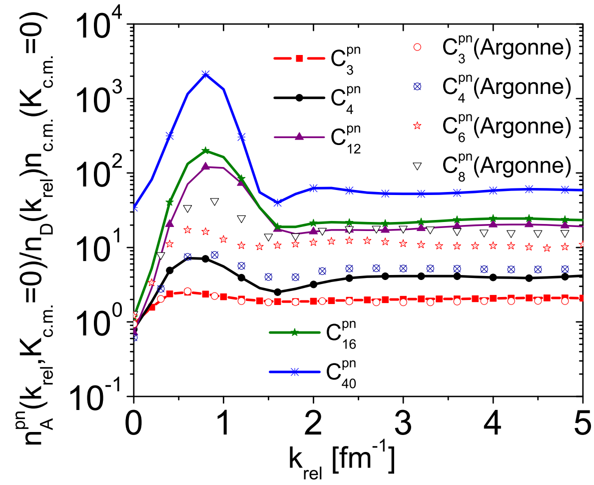

FIG. 8. Determining the constant C_A^{pn} by a plot of Eq. (12) vs k_{rel} with a fixed value of $K_{\mathrm{c.m.}} = 0$. The constant value of Eq. (12) determines the value of C_A^{pn}. For ^{3}He, ^{4}He, ^{6}Li, and ^{8}Be the results obtained with the Argonne momentum distributions [11] are also shown.

nuclei $n^{pn}_{\mathrm{c.m.}} \simeq n^{pp}_{\mathrm{c.m.}}$, the A dependence of $n_A^{pn(\mathrm{fact})}$ is given only by the A dependence of both the constant C_A^{pn} and the c.m. momentum distribution $n^{pn}_{\mathrm{c.m.}}$, with the former determining the amplitude of $n_A^{pn(\mathrm{fact})}(k_{\mathrm{rel}}, K_{\mathrm{c.m.}} = 0)$ and the latter its damping with increasing values of $K_{\mathrm{c.m.}}$. This is clearly shown in Figs. 1–5, where it can indeed be seen that the decrease in $n_A^{pn}(k_{\mathrm{rel}}, K_{\mathrm{c.m.}})$ at $k_{\mathrm{rel}} > k^-_{\mathrm{rel}}$ exactly follows the rate of decrease of $n_A^{pn}(K_{\mathrm{c.m.}})$ shown in Fig. 6, whose low $K_{\mathrm{c.m.}}$ distribution coincides with $n^{pn}_{\mathrm{c.m.}}(K_{\mathrm{c.m.}})$. Therefore it can be concluded that C_A^{pn} (i) is independent of k_{rel} and $K_{\mathrm{c.m.}}$, i.e., it is a quantity depending only upon the value of A, (ii) it is not a free and adjustable parameter, but a quantity resulting from *ab initio* many-body calculations of the momentum distributions, since (iii) it is defined in terms of the magnitude of $n_A^{pn}(k_{\mathrm{rel}}, K_{\mathrm{c.m.}} = 0)$ at $k_{\mathrm{rel}} \gtrsim k^-_{\mathrm{rel}}$, the deuteron momentum distribution, and, eventually, by the c.m. momentum distribution of the pair, i.e., by quantities resulting from many-body calculations and from the factorization property of the momentum distributions. To sum up, the value of C_A^{pn} is given by the following relation:

$$\lim_{k_{\mathrm{rel}} > k^-_{\mathrm{rel}}} \frac{n_A^{pn}(k_{\mathrm{rel}}, K_{\mathrm{c.m.}} = 0)}{n^{pn}_{\mathrm{c.m.}}(K_{\mathrm{c.m.}} = 0)\, n_D(k_{\mathrm{rel}})} = \mathrm{Const} \equiv C_A^{pn}. \quad (12)$$

The validity of Eq. (12) and the determination of the value of C_A^{pn} are illustrated in Fig. 8. It can be seen that at low values of the relative momentum ($k_{\mathrm{rel}} \lesssim 1.5$ fm^{-1}) the ratio. Eq. (12), exhibits a strong dependence upon k_{rel}, reflecting the A-dependent mean-field structure, whereas, starting from $k_{\mathrm{rel}} \simeq 2$–$2.5$ fm^{-1}, a constant behavior is observed for all values of A that have been considered; in particular, in the case of $A = 3$ and $A = 4$, for which accurate wave functions have been used, the consistency with a constant value is very good, whereas for complex nuclei, which are more sensitive to many-body approximations, the error in the determination of the value of C_A^{pn} is higher. The obtained values of C_A^{pn} are listed in Table I, where the values obtained with the VMC results of

TABLE I. Values of the constant C_A^{pn} [Eq. (12)] extracted from Fig. 8, with the error determined according to the expression $C_A^{pn} = \frac{(C_A^{pn})^{\rm Max}+(C_A^{pn})^{\rm Min}}{2} \pm \frac{(C_A^{pn})^{\rm Max}-(C_A^{pn})^{\rm Min}}{2}$, where $(C_A^{pn})^{\rm Max}$ and $(C_A^{pn})^{\rm Min}$ are determined in the region of $k_{\rm rel} \geqslant 3.0$ fm^{-1}. Values in parentheses were obtained using the VMC wave function from Ref. [11].

^{2}H	^{3}He	^{4}He	^{6}Li	^{8}Be	^{12}C	^{16}O	^{40}Ca
1.0	2.0 ± 0.1	4.0 ± 0.1	–	–	20 ± 1.6	24 ± 1.8	60 ± 4.0
1.0	(2.0 ± 0.1)	(5.0 ± 0.1)	(11.1 ± 1.3)	(16.5 ± 1.5)	(–)	(–)	(–)

Ref. [11] are also shown in parentheses. The difference in the value of $C_{A=4}^{pn}$ between ours and the VMC approaches could be attributed to the different Hamiltonian (V8′ NN interaction in our case and AV18 in VMC method) and to the different variational wave functions, whereas in the case of heavier nuclei possible effects from the omitted terms of the cluster expansion should also be considered. All of these possibilities are under investigation. Nonetheless, the results of both approaches exhibit the same A dependency, i.e., an increase in the value of C_A^{pn} with the value of A, which confirms the factorization property of the momentum distribution and which can be explained with the very physical meaning of C_A^{pn}. As a matter of fact Eq. (10) provides the physical meaning of the constant C_A^{pn}, namely, in the factorization region one obtains

$$\begin{aligned} n_{pn}^{\rm SRC,BB}(K_{\rm c.m.}=0) &= \int_{k_{\rm rel}^-=1.5}^{\infty} d\,\mathbf{k}_{\rm rel} \int_0^{\infty} n_A^{pn}(\mathbf{k}_{\rm rel},\mathbf{K}_{\rm c.m.})\delta(\mathbf{K}_{\rm c.m.})\,d\,\mathbf{K}_{\rm c.m.} \\ &\simeq C_A^{pn}\, n_{\rm c.m.}^{pn}(K_{\rm c.m}=0)\,4\pi \int_{k_{\rm rel}^-=1.5}^{\infty} n_D(k_{\rm rel})k_{\rm rel}^2\,dk_{\rm rel}, \end{aligned} \quad (13)$$

which represents the momentum distribution of back-to back nucleons integrated in the region of relative momentum $k_{\rm rel} \geqslant 1.5$ fm^{-1}. Thus C_A^{pn} represent a measure of the number of SRCd pn pairs with c.m. momentum distribution $n_{\rm c.m.}^{pn}(K_{\rm c.m.}=0)$, i.e., the number of deuteron-like pairs. At the same time the equation

$$\begin{aligned} N_{pn}^{\rm SRC} &= \int_0^{K_{\rm c.m.}^{\rm max}} d\,\mathbf{K}_{\rm c.m.} \int_{k_{\rm rel}(K_{\rm c.m.})}^{\infty} n_A^{pn}(\mathbf{k}_{\rm rel},\mathbf{K}_{\rm c.m.})d\,\mathbf{k}_{\rm rel} \\ &\simeq C_A^{pn}\,(4\pi)^2 \int_0^{K_{\rm c.m.}^{\rm max}} n_{\rm c.m.}^{pn}(K_{\rm c.m.})\,K_{\rm c.m.}^2\,d\,K_{\rm c.m.} \\ &\quad \times \int_{k_{\rm rel}^-(K_{\rm c.m.})}^{\infty} n_D(k_{\rm rel})\,k_{\rm rel}^2\,d\,k_{\rm rel} \end{aligned} \quad (14)$$

represents the number of SRCd pn pairs in the entire two-nucleon SRC region, characterized by $K_{\rm c.m}^{\rm max} \lesssim 1$–$1.5$ fm^{-1} and $k_{\rm rel}^- \gtrsim 1.5$ fm^{-1}.[4]

[4]Following the original suggestion in Ref. [18] we also adopt here the region $k_{\rm rel}^- \gtrsim 1.5$ fm^{-1} as the *SRC region*, although, more correctly, based on the results of many-body calculations, the SRC region starts from $k_{\rm rel}^- \gtrsim 2$ fm^{-1}.

IV. THE FACTORIZATION PROPERTY OF THE NUCLEAR WAVE FUNCTION AND THE HIGH-MOMENTUM BEHAVIOR OF THE MOMENTUM DISTRIBUTIONS

A. SRCs as a result of wave-function factorization

It has been demonstrated that the the momentum distributions of nuclei in the region of SRCs are governed by the *factorization property* of the nuclear wave function at short internucleon distances, described by the relation

$$\lim_{r_{ij}\to 0} \Psi_0(\{\boldsymbol{r}\}_A) \simeq \hat{\mathcal{A}} \left\{ \chi_o(\boldsymbol{R}_{ij}) \sum_{n,f_{A-2}} a_{o,n,f_{A-2}} [\Phi_n(\boldsymbol{x}_{ij},\boldsymbol{r}_{ij}) \oplus \Psi_{f_{A-2}}(\{\boldsymbol{x}\}_{A-2},\{\boldsymbol{r}\}_{A-2})] \right\}, \quad (15)$$

where (i) $\{\boldsymbol{r}\}_A$ and $\{\boldsymbol{r}\}_{A-2}$ denote the set of radial coordinates of nuclei A and $A-2$, respectively; (ii) $\boldsymbol{r}_{ij}$ and $\boldsymbol{R}_{ij}$ are the relative and c.m. coordinate of the nucleon pair ij, described by the relative wave function Φ_n and the c.m. wave function χ_o in the 0s state; and (iii) $\{\boldsymbol{x}\}_{A-2}$ and $\boldsymbol{x}_{ij}$ denote the set of spin-isospin coordinates of the nucleus $(A-2)$ and the pair (ij). Equation (15) has been introduced in Ref. [25], demonstrating that the SRCd nuclear two-nucleon momentum distribution factorizes into the vector-coupled product of the relative and c.m. momentum distribution of an NN pair. In particular, in Ref. [24] the factorization property of the nuclear wave function has been shown to hold in the case of *ab initio* wave functions of few-nucleon systems, showing that the momentum-space wave function of ^{3}He and ^{4}He factorize in the region of *high* ($k_{\rm rel}^- \gtrsim 2$ fm^{-1}) relative momenta coupled to *low* c.m. momenta ($K_{\rm c.m.} \lesssim 1.0$ fm^{-1}), whereas at higher values of $K_{\rm c.m.}$ factorization still occurs but starting at increasing values of $k_{\rm rel}$. This behavior indeed appears in Figs. 1(a)–5(a), in the case of both few-nucleon systems and complex nuclei. Finally, in Ref. [23], the factorization property of the wave function and momentum distribution has also been shown to occur in the case of nuclear matter treated within the Brueckner-Bethe-Goldstone approach. In order to provide new evidence about the validity of the factorization property, we show in Figs. 9 and 10 the ratio of the factorized momentum distribution of a pn pair, Eq. (10), to the exact momentum distribution, $n_A^{pn}(k_{\rm rel},K_{\rm c.m.},\Theta)$, i.e., the quantity

$$R_{\rm fact/exact}^{pn} = \frac{C_A^{pn}\,n_D(k_{\rm rel})n_{\rm c.m.}^{pn}(K_{\rm c.m.})}{n_A^{pn}(k_{\rm rel},K_{\rm c.m.},\Theta)} \quad (16)$$

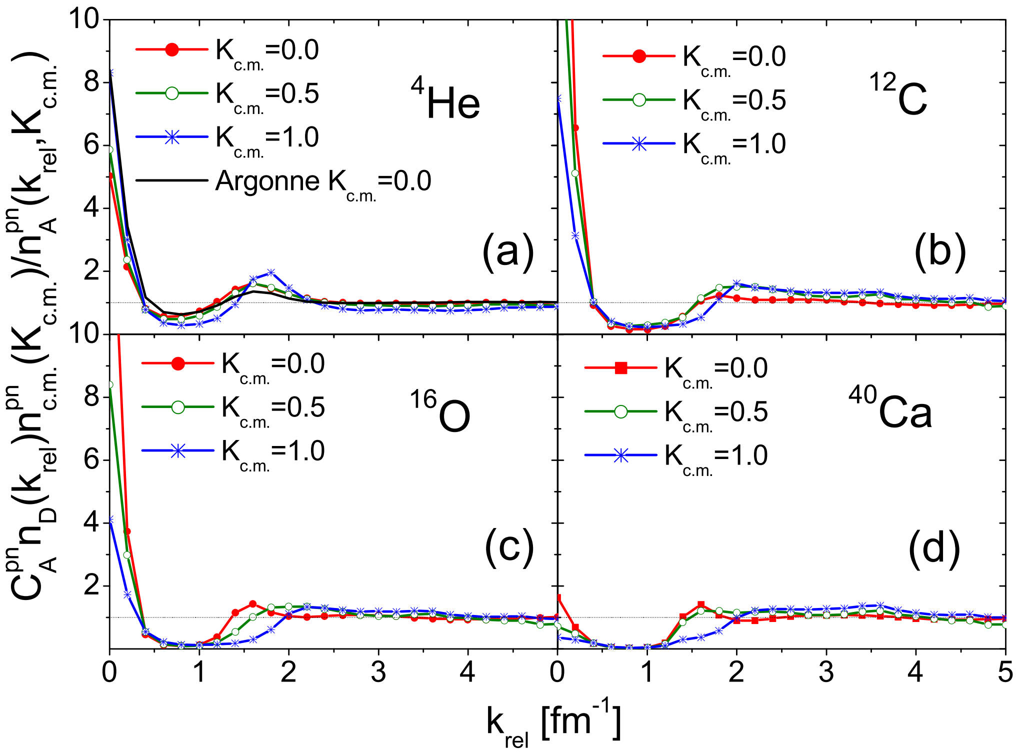

FIG. 9. Ratio [Eq. (16)] between the factorized distributions [Eq. (10)] and the exact ones ($\Theta = 0^\circ$) for ^{4}He, ^{12}C, ^{16}O, and ^{40}Ca in correspondence to $K_{\rm c.m.} = 0$, 0.5, and 1 fm^{-1}. For ^{4}He the results obtained with the Argonne momentum distributions [11] are shown by the solid line.

plotted on a linear scale. It can be seen that, independently of the nuclear mass and the values of $K_{\rm c.m.}$, the ratio exhibits, at $k_{\rm rel}^{-} \gtrsim 2$ fm^{-1}, a constant value equal to one. The scaling to 1 is perfect for $A = 4,6,8$ nuclei for which *ab initio* VMC momentum distributions have been used, whereas it presents small oscillations for complex nuclei, a behavior that should be attributed to the approximations which have been used to solve the many-body problem.

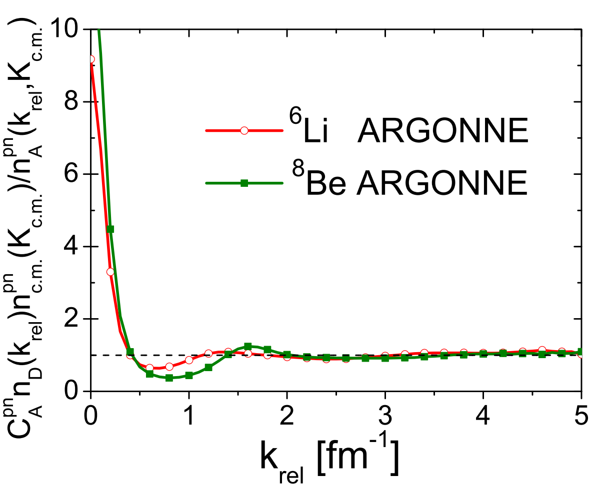

FIG. 10. Ratio [Eq. (16)] between the factorized distributions, Eq. (10), and the exact ones for ^{6}Li and ^{8}Be, corresponding to $K_{\rm c.m.}$=0, obtained with the Argonne VMC wave functions [11].

B. Wave-function factorization and the relation between the relative momentum distribution of *pn* pairs in nuclei and the deuteron momentum distributions

In Fig. 11 the two-nucleon momentum distributions of *pn* pairs in nuclei is compared with the deuteron momentum distribution. As already pointed out, the in-medium *pn* momentum distribution is a relevant quantity for the study of in-medium dynamics since it represents a unique opportunity to compare the properties of a free bound *pn* system with the properties of a *pn* system embedded in the medium. The ratio

$$R_{pn/D}(k_{\rm rel}, K_{\rm c.m.} = 0) = \frac{n_A^{pn}(k_{\rm rel}, K_{\rm c.m.} = 0)}{C_A^{pn} n_{\rm c.m.}^{pn}(K_{\rm c.m.} = 0)} \qquad (17)$$

is presented in Fig. 11(a), whereas the quantity

$$R_{pn/D}(k_{\rm rel}) = \frac{n_A^{pn}(k_{\rm rel})}{C_A^{pn}} \qquad (18)$$

is shown in Figs. 11(b)–11(d). The scaling of Eq. (17) to the deuteron momentum distributions, starting from $k_{\rm rel} \simeq 2$ fm^{-1}, is clearly exhibited and it can also be seen that scaling of $n_A^{pn}(k_{\rm rel})$ also takes place [cf. Eq (18)], but only at very large values of $k_{\rm rel} \gtrsim 4$ fm^{-1}. These results are obtained both with our momentum distributions and with the VMC ones. Comparing Figs. 11(a) and 11(b) it can be concluded that the *pn* momentum distribution in nuclei is governed, at a high value of the relative momentum, only by the deuteron-like momentum components, i.e., by the two-nucleon momentum distributions with $K_{\rm c.m.} = 0$.

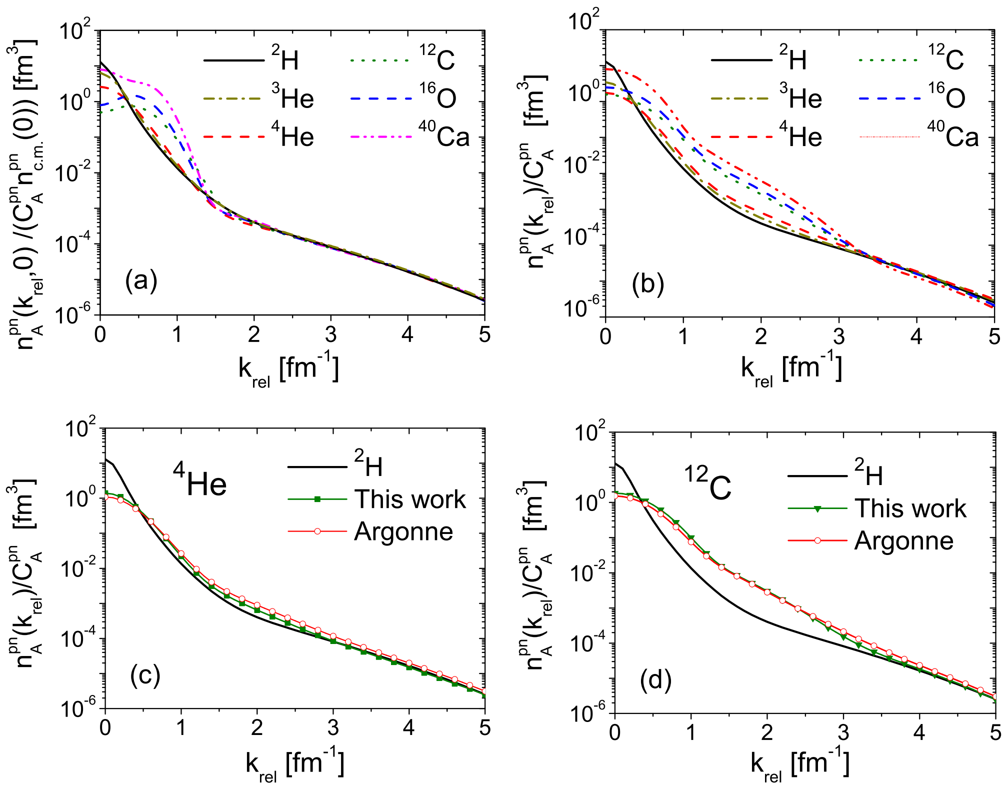

FIG. 11. (a), (b) Comparison of the deuteron momentum distributions with the two-nucleon momentum distributions of various nuclei obtained in the present paper. (a) The validity of the relation $n_A^{pn}(k_{\rm rel},K_{\rm c.m.})/C_A^{pn} n_{\rm c.m.}^{pn}(K_{\rm c.m.}=0) \simeq n_D(k_{\rm rel})$, when $K_{\rm c.m.}=0$ and $k_{\rm rel} \gtrsim\sim 2\,{\rm fm}^{-1}$, is demonstrated. (b) Demonstration that when the $K_{\rm c.m.}$-integrated two-nucleon momentum distributions are considered, the relation $n_A^{pn}(k_{\rm rel})/C_A^{pn} \simeq n_D(k_{\rm rel})$ is also valid, but only at $k_{\rm rel} \geqslant 3.5$–4 fm^{-1}. (c), (d) The quantity $n_A^{pn}(k_{\rm rel})/C_A^{pn}$ for ^{4}He (c) and ^{12}C corresponding to the momentum distributions obtained in the present paper and in Ref. [11]. In (c) and (d) the values of C_A^{pn} are the ones listed in Table I. These results unambiguously prove that both $n_A^{pn}(k_{\rm rel},K_{\rm c.m.}=0)$ and $n_A^{pn}(k_{\rm rel})$ do factorize to the deuteron momentum distribution, but starting at appreciably different values of $k_{\rm rel}$ in the two cases. These results also show that $n_A^{pn}(k_{\rm rel})$ at $k_{\rm rel} \geqslant 3.5$–4 fm^{-1} is mainly governed by back-to-back pn pairs.

C. Wave-function factorization and the relation between the one-nucleon and the two-nucleon momentum distributions. The one-nucleon momentum distribution vs the deuteron momentum distribution

The results presented in Figs. 9 and 10 represent unquestionable evidence of the validity of the factorization property, which leads to the convolution model (CONV) of the one-nucleon spectral function and momentum distributions describing both quantities in terms of a convolution integral of the relative and c.m. momentum distributions of a correlated pair [25]. Within the CONV the exact relation between the one- and the two-nucleon momentum distributions, namely (e.g., for protons),

$$n_A^p(\mathbf{k}_1) = \frac{1}{A-1}\left(\int n_A^{pn}(\mathbf{k}_1,\mathbf{k}_2)\,d\,\mathbf{k}_2 + 2\int n_A^{pp}(\mathbf{k}_1,\mathbf{k}_2)\,d\,\mathbf{k}_2\right), \tag{19}$$

is represented in the *correlation region* at high momenta by the following convolution integrals [$\mathbf{k}_1+\mathbf{k}_2+\mathbf{k}_3=0$, $\mathbf{k}_3=\mathbf{K}_{A-2}=-\mathbf{K}_{\rm c.m.}=-(\mathbf{k}_1+\mathbf{k}_2)$]:

$$n_A^p(\mathbf{k}_1) = \int n_{\rm rel}^{pn}\left(\left|\mathbf{k}_1-\frac{\mathbf{K}_{\rm c.m.}}{2}\right|\right) n_{\rm c.m.}^{pn}(\mathbf{K}_{\rm c.m.})\,d\,\mathbf{K}_{\rm c.m.} + 2\int n_{\rm rel}^{pp}\left(\left|\mathbf{k}_1-\frac{\mathbf{K}_{\rm c.m.}}{2}\right|\right) n_{\rm c.m.}^{pp}(\mathbf{K}_{\rm c.m.})\,d\,\mathbf{K}_{\rm c.m.}. \tag{20}$$

Equation (20) establishes a relation between the one-nucleon momentum distribution $n_A^p(\mathbf{k}_1)$ and the relative and c.m. momentum distributions of the N_1N_2 pair.[5] At large values of $\mathbf{k}_1$, such that $\boldsymbol{k}_1 \gg \boldsymbol{K}_{\rm c.m.}/2$, the convolution formula, could in principle be approximated by

$$n_A^p(k_1) \simeq n_{\rm rel}^{pn}(k_{\rm rel}=k_1) + 2n_{\rm rel}^{pp}(k_{\rm rel}=k_1), \tag{21}$$

which represents the contribution of BB nucleons to the one-nucleon momentum distribution. Equation (21) can also be

[5]In actual calculations in Ref. [25] the exact Eq. (20) has been approximated using an effective two-nucleon momentum distribution.

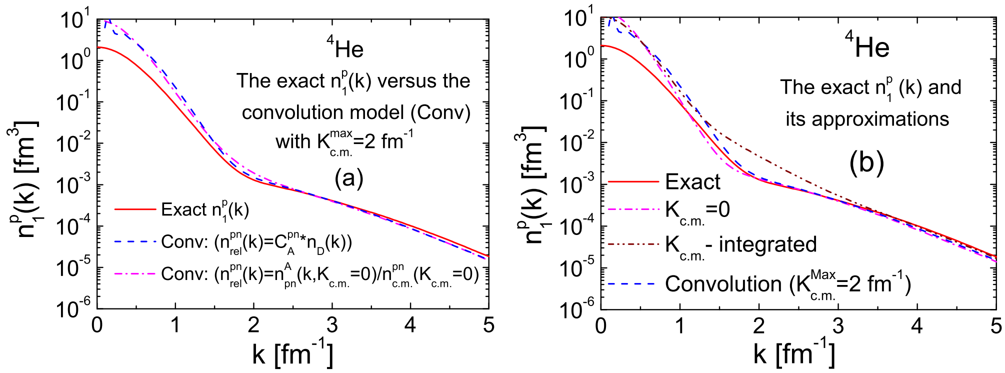

FIG. 12. (a) The exact proton momentum distribution $n_A^p(k)$ ($k_1 \equiv k$) compared with the convolution model, Eq. (21) (Conv), calculated with two different expressions for $n_{\rm rel}^{pn}$. (b) The exact $n_A^p(k)$ compared with (i) the asymptotic approximation of the convolution model [Eqs. (21) and (22)] ($K_{\rm c.m.}=0$); (ii) Eq. (21) with $n_{\rm rel}^{N_1N_2}(k_1=k_{\rm rel})$ replaced by the $K_{\rm c.m.}$-integrated relative momentum distributions $n_A^{N_1N_2}(k_{\rm rel}) = \int n_A^{N_1N_2}(\mathbf{k}_{\rm rel},\mathbf{K}_{\rm c.m.})\, d\,\mathbf{K}_{\rm c.m.}$; and (iii) the convolution model [Eq. (24)] as in (a).

expressed in the equivalent form

$$n_A^p(k_1) = \frac{n_A^{pn}(k_{\rm rel}=k_1,K_{\rm c.m.}=0)}{n_{\rm c.m.}^{pn}(K_{\rm c.m.}=0)} + 2\frac{n_A^{pp}(k_{\rm rel}=k_1,K_{\rm c.m.}=0)}{n_{\rm c.m.}^{pp}(K_{\rm c.m.}=0)} \tag{22}$$

as well as in the form

$$n_A^p(k_1) \simeq C_A^{pn} n_D(k_{\rm rel}=k_1) + 2\frac{n_A^{pp}(k_{\rm rel}=k_1,K_{\rm c.m.}=0)}{n_{\rm c.m.}^{pp}(K_{\rm c.m.}=0)}, \tag{23}$$

which establishes a clear-cut relation between the one-nucleon momentum distribution and the momentum distribution of the deuteron in the case of pairs of nucleons with BB ($K_{\rm c.m.}=0$) momenta.[6] Starting from a factorized wave function, a relation similar to Eq. (21) has been obtained in Ref. [39], where, however, instead of the relative momentum distribution $n_{\rm rel}^{N_1N_2}(k_{\rm rel}) = n_A^{N_1N_2}(k_{\rm rel}=k_1,K_{\rm c.m.}=0)/n_{\rm c.m.}^{N_1N_2}(K_{\rm c.m.}=0)$, the $K_{\rm c.m.}$-integrated relative momentum distribution [Eq. (7)] has been used. We show that, as expected from Figs. 11(a) and 11(b), the relation between the one- and the two-body momentum distribution will be numerically different. Let us first analyze the validity of the convolution model. In Fig. 12 a detailed analysis of the model is presented for the ^{4}He nucleus. The following features *in the region of factorization dominated by SRCs* ($k \gtrsim 2$ fm^{-1}) are worth stressing: (i) The exact momentum distribution n_A^p is correctly approximated by the convolution formula [Eq. (20)] and, particularly, by its asymptotic behavior [Eq. (21)], including its deuteron-like character for the pn distribution, i.e., for back-to-back SRCd nucleon pairs. (ii) The exact calculation, the calculation with the convolution formula, using there either $C_A^{pn} n_D(k_{\rm rel})$ or $n_A^{pn}(k_{\rm rel},K_{\rm c.m.}=0)/n_{\rm c.m.}^{pn}(K_{\rm c.m.}=0)$ for the relative motion, yields very similar results starting from $k_{\rm rel} \gtrsim 2\,{\rm fm}^{-1}$, whereas Eq. (21) with the $\mathbf{K}_{\rm c.m.}$-integrated relative momentum distribution reproduces $n_A^p(k)$ only when $k_{\rm rel} \gtrsim$ 3.5–4 fm^{-1}. In order to further demonstrate the relationships of the one- and two-nucleon momentum distributions we show in Fig. 13 the ratios

$$R_{N_1N_2/N_1}^{\rm BB}(k_1) = \frac{1}{n_A^p(k)}\left[\frac{n_A^{pn}(k_{\rm rel},K_{\rm c.m.}=0)}{n_{\rm c.m.}^{pn}(K_{\rm c.m.=0})} + 2\frac{n_A^{pp}(k_{\rm rel},K_{\rm c.m.}=0)}{n_{\rm c.m.}^{pp}(K_{\rm c.m.=0})}\right] \tag{24}$$

and

$$R_{N_1N_2/N_1}^{\rm int}(k_1) = \frac{n_A^{pn}(k_{\rm rel}) + 2n_A^{pp}(k_{\rm rel})}{n_A^p(k_1)}, \tag{25}$$

where in both quantities n_A^p is the exact proton momentum distribution and the numerators differ in that in Eq. (24) BB nucleon distributions are considered, unlike the case of Eq. (25), where the $\mathbf{K}_{\rm c.m.}$-integrated relative momentum distributions are adopted. The regions of validity of the two cases, both corresponding to $k_1 \simeq k_{\rm rel}$, i.e., $K_{\rm c.m.} \simeq 0$ are determined by a constant value of the ratios. As expected from the results presented in Figs. 11 and 12, Eq. (24) is unity over a wider range of momenta. The results presented in Fig. 13 provide further evidence of the validity of both the factorization property and the convolution model and tell us that when the ratio equals 1, the one-nucleon momentum distribution is dominated by BB configurations with $\mathbf{k}_1 = -\mathbf{k}_2 = \mathbf{k}_{\rm rel}$, $\mathbf{K}_{\rm c.m.}=0$. Concerning the relationship of the one-nucleon momentum distributions and the momentum distributions of the deuteron, as already illustrated, this is given by Eq. (23). However, by plotting the ratio of the one-nucleon momentum distribution to the momentum distributions of the deuteron $R_{A/D}(k_1) = \frac{n_A^p(k_1)}{n_D(k_1)}$ the relationships between the two quantities can be exhibited in more detail, as quantitatively illustrated in Ref. [17]. There it has been shown that $N_{A/D}(k_1)$ never becomes constant, which means that $n_1^A(k_1)$ is not linearly proportional to $n_D(k_1)$; this is mostly due to the contribution of the pp distribution, which increases with increasing momentum k_1, and to the c.m. motion of a pn pair in the nucleus. Only if pp contributions are disregarded and only back-to-back pn pairs considered does one indeed

[6]Note that in the following, we use $n_{\rm c.m.}^{pp}(K_{\rm c.m.}) = n_{\rm c.m.}^{pn}(K_{\rm c.m.})$.

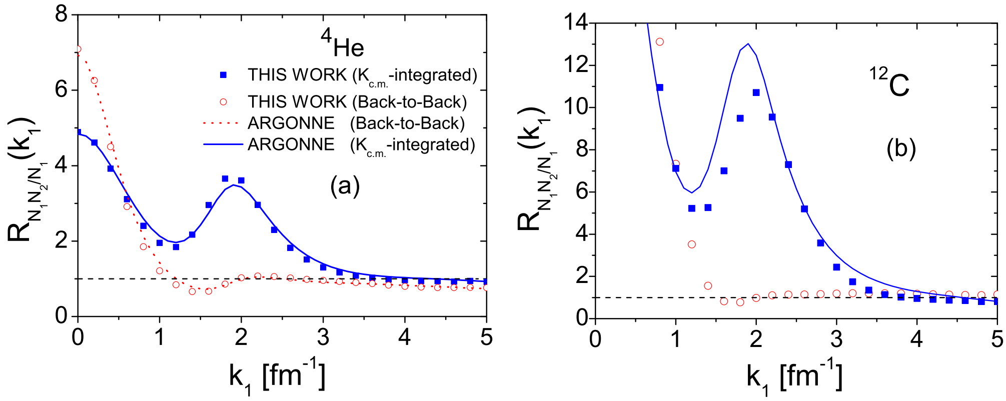

FIG. 13. Ratio of the full two-nucleon momentum distribution $n_{pn} + 2n_{pp}$ to the one-nucleon momentum distribution n_A^p for ^{4}He (a) and ^{12}C (b) calculated using in the numerator the relative two-nucleon distributions $n_A^{pn}(k_{\rm rel} = k_1, K_{\rm c.m.} = 0)/n_{\rm c.m.}(K_{\rm c.m.} = 0)$ [Eq. (24); open circles] and the $\mathbf{K}_{\rm c.m.}$-integrated two-nucleon momentum distributions $n_A^{pn}(k_{\rm rel})$ [Eq. (25); filled squares]; in both cases the denominator is the one-nucleon momentum distribution. The solid line denotes the results obtained with the Argonne VMC wave function [11].

obtain that in the region $k_1 \gtrsim 2$ fm^{-1}, $n_A^p(k_1) \simeq C_A^{pn} n_D(k_1)$. The relation between the nucleon momentum distribution of nucleus A and the deuteron momentum distribution has been and is still being used in the treatment of SRCs. Still now the proportionality of the nuclear momentum distribution to the momentum distribution of the deuteron is sometimes assumed, which is equivalent to the statement that the high-momentum content of the nucleus is fully determined by the two-nucleon state (ST) = (10). In the past realistic calculations of the nuclear momentum distributions at high momenta could not be performed with sufficient accuracy and the similarity of the deuteron and the nuclear momentum distribution has been simply assumed, e.g., in the early VMC calculations [42] or in the development of workable models of the spectral function for complex nuclei [25]. Recent advanced calculations of the one- and two-body momentum distributions [3,10,11,16,17], including the results of the present paper, show that also states different from the deuteron one, namely, states (01) and (11), do contribute to the high-momentum part of the momentum distributions, demonstrating, in the case of state (11), that a considerable number of two-nucleon states with an odd value of the relative orbital momentum is present in the realistic ground-state wave function of nuclei.

D. Wave-function factorization and the nuclear contacts

The concept of *contact*, introduced by Tan in Ref. [38], to describe the short-range behavior of two unlike electrons in a two-component Fermi gas, has recently been discussed within the context of SRCs in nuclei (see, e.g., Refs. [39,40]). Although a detailed discussion of this topic is outside the aim of the present paper and will be discussed elsewhere, it is nevertheless useful to stress here that (i) the *contacts* are quantities that measure the probability of finding two particles at short relative distances [38,39], and (ii) they are obtained, in both atomic and nuclear systems, by postulating a factorized wave function of the form of Eq. (15) [39]. For these reasons, the quantity C_A^{pn} we have obtained, measuring the probability of having SRCd back-to-back pn pairs, represents nuclear pn contacts.[7]

V. ON THE NUMBER OF HIGH-MOMENTUM SHORT-RANGE CORRELATED NUCLEON-NUCLEON PAIRS IN NUCLEI

Having at our disposal the two-nucleon momentum distributions, the absolute values of the number of SRCd pairs, i.e., the integral of the two-nucleon momentum distributions in a given relative and c.m. momentum region, can be calculated and, as in the case of the deuteron, a proper definition of the probability of SRCs in a nucleus can be given. However, in a complex nucleus the two-nucleon momentum distributions depend upon three variables so that, as pointed out in Ref. [17], there is a certain degree of ambiguity in providing a clear-cut definition of the probability of SRCs in terms of an integral of the two-nucleon momentum distributions. In the case of the deuteron, which is described only in terms of a back-to-back configuration ($\boldsymbol{k}_1 = -\boldsymbol{k}_2 = \boldsymbol{k}$, $\boldsymbol{k}_{\rm rel} \equiv \boldsymbol{k}$, $\boldsymbol{K}_{\rm c.m.} = 0$), a commonly adopted definition of the probability of SRCs is given by the integral of the momentum distribution $n_D(k)$ ($k_{\rm rel} \equiv k$) in the interval $1.5 \leqslant k \leqslant \infty$ fm^{-1}, which is the region dominated by the high-momentum components generated by the repulsive core and by the deuteron D wave produced by the tensor force. Therefore in the deuteron the total number of pn pairs is $N_D = 1$, and the number of BB SRCd pn pairs is

$$N_D^{\rm BB} = 4\pi \int_{k^-=1.5}^{\infty} n_D(k)\, k^2\, d\,k \equiv N_{pn}^{\rm BB} =\simeq 0.036, \quad (26)$$

i.e., only 4% of the pn pair is SRCd (this percentage corresponds to the AV18 interaction). The extent to which

[7]It should be stressed that in the case of nuclei four contacts, depending upon the spin-isospin state of the pair, can be defined; moreover, the contacts may be defined to depend upon the center of mass of the correlated pair, namely, for a fixed value of the c.m. momentum, for back-to-back nucleons, and for the $\mathbf{K}_{\rm c.m.}$-integrated momentum distributions.

TABLE II. Number of back-to-back (BB) proton-neutron (pn), and proton-proton (pp) pairs [Eq. (27)], integrated momentum distribution of BB SRCd pairs [Eq. (28)], and percentage probability $\mathcal{P}^{\mathrm{SRC,BB}}_{N_1N_2} = 100\, N^{\mathrm{SRC,BB}}_{N_1N_2}/N^{\mathrm{BB}}_{N_1N_2}$. Microscopic wave functions corresponding to the AV18 interaction [35], for ^{2}H and ^{3}He [32,33], and to the AV8′ interaction [36], for ^{4}He [34] and complex nuclei [15]. Values in parentheses were obtained with the VMC momentum distributions from Ref. [11], which were calculated with the AV18 + UX interaction.

	$N^{\mathrm{BB}}_{N_1N_2}$	$N^{\mathrm{SRC,BB}}_{D}$	$\mathcal{P}^{\mathrm{SRC,BB}}_{D}$	$N^{\mathrm{BB}}_{N_1N_2}$	$N^{\mathrm{SRC,BB}}_{N_1N_2}$	$\mathcal{P}^{\mathrm{SRC,BB}}_{N_1N_2}$	$N^{\mathrm{BB}}_{N_1N_2}$	$N^{\mathrm{SRC,BB}}_{N_1N_2}$	$\mathcal{P}^{\mathrm{SRC,BB}}_{N_1N_2}$
		^{2}He			^{3}He			^{4}He	
pn	1	0.036	3.6	6.22	0.22	3.5	2.54	0.08	3.1
	(1)	(0.036)	(3.6)	(5.82)	(0.20)	(3.4)	(2.05)	(0.09)	(4.3)
pp	–	–	–	2.05	0.01	0.5	0.55	0.005	0.9
	–	–	–	(2.10)	(0.01)	(0.5)	(0.42)	(0.004)	(1.0)
		^{12}C			^{16}O			^{40}Ca	
pn	3.80	0.08	2.1	7.32	0.11	1.5	59.07	0.24	0.4
pp	1.72	0.01	0.6	3.27	0.01	0.4	27.61	0.02	0.1

such a probability will differ in a complex nucleus is a relevant issue, for it can provide information on in-medium effects on short-range pn dynamics. For this reason, a similar definition, i.e., the integral of the relative momentum distribution in the range $k_{\mathrm{rel}} \gtrsim 1.5\ \mathrm{fm}^{-1}$, might also be introduced in the case of a complex nucleus, keeping in mind, however, that in a nucleus all possible values of $K_{\mathrm{c.m.}}$ and Θ, as well as all four spin-isospin (ST) values of the pair [mostly (10), (01), and (11)], contribute to the momentum distributions, as demonstrated in Refs. [7,8,11,17] .

We consider the following quantities:

(1) The total number of back-to-back N_1N_2 pairs, $N^{\mathrm{BB}}_{N_1N_2}(K_{\mathrm{c.m.}}=0)$, resulting from the integration of the pair relative momentum and the total number of *short-range correlated back-to-back* N_1N_2 pairs, $N^{\mathrm{SRC,BB}}_{N_1N_2}(K_{\mathrm{c.m.}}=0, k_{\mathrm{rel}} \geqslant 1.5)$, which are given, respectively, by

$$\begin{aligned} N^{\mathrm{BB}}_{N_1N_2}&(K_{\mathrm{c.m.}}=0) \\ &= 4\pi \int_0^\infty n_A^{N_1N_2}(k_{\mathrm{rel}}, K_{\mathrm{c.m.}}=0)\, k_{\mathrm{rel}}^2\, dk_{\mathrm{rel}} \\ &\equiv N^{\mathrm{BB}}_{N_1N_2}, \end{aligned} \tag{27}$$

$$\begin{aligned} N^{\mathrm{SRC,BB}}_{N_1N_2}&(K_{\mathrm{c.m.}}=0, k_{\mathrm{rel}} \geqslant 1.5) \\ &= 4\pi \int_{1.5}^\infty n_A^{N_1N_2}(k_{\mathrm{rel}}, K_{\mathrm{c.m.}}=0)\, k_{\mathrm{rel}}^2\, dk_{\mathrm{rel}} \\ &\equiv N^{\mathrm{SRC,BB}}_{N_1N_2}. \end{aligned} \tag{28}$$

In both Eqs. (27) and (28), whose values are shown in Table II, the quantity $n_A^{N_1N_2}(k_{\mathrm{rel}}, K_{\mathrm{c.m.}}=0)$ is the one shown in Figs. 1–5.[8] It can be seen in Table II that for nuclei with $A > 4$ an appreciable decrease in the percentage probabilities $\mathcal{P}^{\mathrm{SRC,BB}}_{N_1N_2}$ of back-to-back proton-neutron (pn) and proton-proton (pp) nucleons does occur with increasing values of A, which can be explained by the similar values of $n_A^{pn}(K_{\mathrm{c.m.}}=0)$ for $A \geqslant 12$ and, at the same time, the substantial increase

[8]Note that Eqs. (27) and (28) have the dimensions of fm^3 provided by the c.m. momentum distribution at $K_{\mathrm{c.m.}}=0$. We call them the *numbers of particles for back-to-back pairs.*

TABLE III. Total number of pairs $N_{N_1N_2}$ [Eq. (30)], total number of SRCd pairs $N^{\mathrm{SRC}}_{N_1N_2}$ [Eq. (29)] [in the case of the deuteron, Eq. (26)], and percentage probability $\mathcal{P}^{\mathrm{SRC,BB}}_{N_1N_2} = 100\, N^{\mathrm{SRC}}_{N_1N_2}/N_{N_1N_2}$. Microscopic wave functions corresponding to the AV18 interaction [35] for ^{2}H and ^{3}He [32,33] and the AV8′ interaction [36] for ^{4}He [34] and complex nuclei [15]. Values in parentheses correspond to the VMC wave functions from Ref. [11].

	$N_{N_1N_2}$	N^{SRC}_{D}	$\mathcal{P}^{\mathrm{SRC}}_{D}(\%)$	$N_{N_1N_2}$	$N^{\mathrm{SRC}}_{N_1N_2}$	$\mathcal{P}^{\mathrm{SRC}}_{N_1N_2}(\%)$	$N_{N_1N_2}$	$N^{\mathrm{SRC}}_{N_1N_2}$	$\mathcal{P}^{\mathrm{SRC}}_{N_1N_2}(\%)$
		^{2}H			^{3}He			^{4}He	
pn	1	0.036	3.6	2	0.093	4.7	4	0.243	6.1
	(1)	(0.036)	(3.6)	–	–	–	–	(0.332)	(8.3)
pp	–	–	–	1	0.025	2.5	1	0.052	5.2
	–	–	–	–	–	–	–	(0.071)	(7.1)
		^{12}C			^{16}O			^{40}Ca	
pn	36	3.02	8.4	64	4.75	7.4	400	21.06	5.3
	–	(3.74)	(10.4)	–	–	–	–	–	–
pp	15	1.22	8.1	28	2.00	7.1	190	9.86	5.2
	–	(1.52)	(10.1)	–	–	–	–	–	–

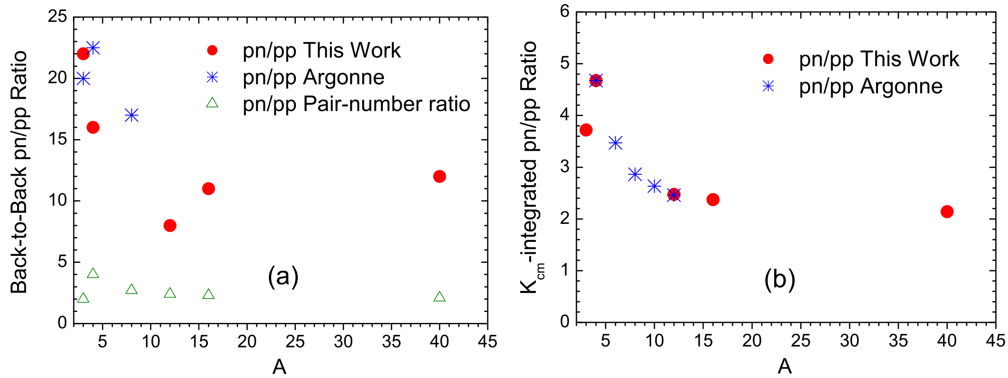

FIG. 14. (a) The ratio $N_{pn}^{\mathrm{SRC,BB}}/N_{pp}^{\mathrm{SRC,BB}}$ using the wave functions of the present work (cf. Table II) and the VMC results from Ref. [11]. (b) The same as (a), for the K_{cm}-integrated momentum distributions (cf. Table III).

in the value of the number of back-to-back proton-neutron and proton-proton nucleons $N_{N_1N_2}^{\mathrm{BB}}$ [Eq. (27)].

(2) The total number of SRCd pairs, defined as the integral in the entire region of variation of $K_{\mathrm{c.m.}}$ and in the region of the relative momentum with $k_{\mathrm{rel}}^{-} \gtrsim 1.5\ \mathrm{fm}^{-1}$, i.e.,

$$\begin{aligned}
N_{N_1N_2}^{\mathrm{SRC}}(k_{\mathrm{rel}}^{-} = 1.5) &= \int_{1.5}^{\infty} d^3\, k_{\mathrm{rel}} \int_0^{\infty} d^3\, K_{\mathrm{c.m.}} n_A^{N_1N_2}(\mathbf{k}_{\mathrm{rel}}, \mathbf{K}_{\mathrm{c.m.}}) \\
&= 4\pi \int_{1.5}^{\infty} k_{\mathrm{rel}}^2\, d\, k_{\mathrm{rel}} n_A^{N_1N_2}(k_{\mathrm{rel}}) \equiv N_{N_1N_2}^{\mathrm{SRC}}. \qquad (29)
\end{aligned}$$

This quantity is compared with the total number of pairs given by

$$N_{N_1N_2} = 4\pi \int_0^{\infty} k_{\mathrm{rel}}^2\, d\, k_{\mathrm{rel}} n_A^{N_1N_2}(k_{\mathrm{rel}}). \qquad (30)$$

The results are listed in Table III. The values of $N_{N_1N_2}^{\mathrm{SRC}}(k_{\mathrm{rel}}^{-} = 1.5)$ include both two-nucleon SRCs (2N SRCs), as well as many-nucleon SRCs generated by the hard high-momentum tail ($K_{\mathrm{c.m.}} \gtrsim 1$) of the c.m. distributions. Note, moreover, that the number of SRCd pairs is the largest in this case since the entire variation of $K_{\mathrm{c.m.}}$ is taken into account; also worth stressing is the almost-constant value of the probability for $A \geqslant 12$, which is due to the same rate of increase in the number of correlated pairs and the total numbers of pN pairs N_{pN}. It is shown in Fig. 11(b) that in the region $1.5 \lesssim k_{\mathrm{rel}} \lesssim 3.5\ \mathrm{fm}^{-1}$ the momentum components with $K_{\mathrm{c.m.}} \neq 0$ are important in $n_A^{pn}(k_{\mathrm{rel}})$. The main results in Tables II and III are summarized in Fig. 14, whose main features should be stressed as follows:

(a) Because of the pn tensor dominance (see Figs. 1–5) the number of SRCd pn pairs in few-nucleon systems and $A < 12$ is larger than the number of pp pairs by a factor of about 20, whereas in medium-weight isoscalar nuclei it is larger by a factor of about 10, to be compared with the factor of 2 ($2Z/(Z-1)$), which is predicted by the naive pair-number ratio.

(b) When the total $\boldsymbol{K}_{\mathrm{c.m.}}$-integrated number of pairs is considered, the value of the pn/pp ratio strongly decreases to a factor of about 2, due to the role played by the c.m. high-momentum components, as can easily be understood by comparing Figs. 1(c) and 2(c) with Figs. 1(d), 2(d), 3(b), and 5(b) with Figs. 3(c) and 5(c).

VI. SHORT-RANGE CORRELATIONS: THEORETICAL PREDICTIONS VS EXPERIMENTAL DATA

Experimental investigation of SRCs is a complicated task, mainly due to the small value of the involved cross sections and the effects of the FSI, which makes it difficult to reconstruct the initial correlated state. Nonetheless, experimental progress has recently been achieved, thanks to the use of intense lepton beams and the development of advanced detector techniques. Nowadays it has become possible to investigate quasielastic $A(e,e'N_1)X$ and $A(e,e'N_1N_2)X$ processes at high values of Q^2 and Bjorken scaling variables $x_B > 1$, a region where (i) the contribution from non-nucleonic degrees of freedom is suppressed, (ii) the effects of initial-state SRCs are emphasized (see Refs. [1–5]), and (iii) the theoretical treatment of the FSI has reached a high degree of sophistication [19–22]. Several SRC properties that have been experimentally investigated deserve a comparison with theoretical calculations, which is presented below.

A. Percentage ratios of different kinds of N_1N_2 pairs in ^{4}He and ^{12}C and their missing momentum dependence

SRCs in ^{4}He and ^{12}C have recently been investigated [26–31] within the following kinematical region:[9] the squared four-momentum transfer $Q^2 \simeq 2\ (\mathrm{GeV}/c)^2$, the Bjorken scaling variable $x_{\mathrm{Bj}} = 1.2$, and the three-momentum transfer $|\mathbf{q}| \equiv q \simeq 1.6\ \mathrm{GeV}/c$. Information on the short-range momentum distribution of correlated pairs has been obtained by the following procedure: triple coincidence processes $^{12}\mathrm{C}(p,p'pN)X$

[9] The same notation as in Ref. [5] is adopted here.

TABLE IV. Percentage ratio of the pn and pp short-range correlated back-to-back (BB) pairs with respect to the total number of correlated pairs and percentage ratio of pp to pn pairs [Eq. (31)] at $k_{\mathrm{rel}} = 2.5\ \mathrm{fm}^{-1}$, calculated using the BB momentum distributions shown in Figs. 1–5. Experimental (expt.) data for ^{12}C are from Refs. [26–29]; experimental data for ^{4}He, from Ref. [30].

	$R_{pn}(\%)$	$R_{pp}(\%)$	$R_{pp/pn}$	$R_{pn}(\%)$	$R_{pp}(\%)$	$R_{pp/pn}$
		^{2}H			^{3}He	
Theor.	100	0	–	89.3	3.16	3.54
Expt.	–	–	–	–	–	–
		^{4}He			^{12}C	
Theor.	93.2	5.43	5.83	96.2	5.01	5.20
Expt.	87.0 ± 14.1	3.9 ± 1.5	5.1 ± 2.6	97.0 ± 22.1	4.8 ± 1.0	5.8 ± 1.5
		^{16}O			^{40}Ca	
Theor.	97.9	5.05	5.15	91.8	6.52	7.11
Expt.	–	–	–	–	–	–

and $^{12}\mathrm{C}(e,e'pN)X$ have been performed by detecting, in coincidence with the struck nucleon, leading protons with a high momentum $\mathbf{p}$ and protons and neutrons moving with recoil momentum $\mathbf{p}_{\mathrm{rec}} = \mathbf{q} - \mathbf{p}$ along a direction that, within the plane-wave impulse approximation, would coincide with the direction opposite the momentum that the struck nucleon had before interaction with the projectile. Specifically, within the PWIA, if before interaction the struck proton had momentum $\mathbf{k}_1$, the leading proton would have momentum $\mathbf{p} = \mathbf{k}_1 + \mathbf{q}$ and the known *missing momentum* would be $\mathbf{p}_m = \mathbf{q} - \mathbf{p} = -\mathbf{k}_1$. Therefore, if the struck proton "1" was the partner of a correlated nucleon "2" with momentum $\mathbf{k}_2 \simeq -\mathbf{k}_1$, in coincidence with the leading proton, a recoiling nucleon "2" with momentum $\mathbf{p}_{\mathrm{rec}} = \mathbf{p}_m = -\mathbf{k}_1 \simeq \mathbf{k}_2$ should be observed along the direction opposite $\mathbf{p}_m$. In Refs. [26–31] the processes $A(p,p'p)X$, $A(e,e'p)X$, $A(p,p'pp)X$, $A(e,e'pn)X$, and $A(e,e'pp)X$ have been investigated by detecting mainly back-to-back pp and pn nucleons in the range $1.5 \lesssim p_m \lesssim 3\ \mathrm{fm}^{-1}$ in ^{12}C and $1.5 \lesssim p_m \lesssim 4\ \mathrm{fm}^{-1}$ in ^{4}He. Within such a kinematic setup, the percentage ratios of the cross sections pertaining to pn and pp pairs have been extracted. Using the two-nucleon relative momentum distributions shown in Figs. 1–5 corresponding to BB nucleons ($K_{\mathrm{c.m.}} = 0$), we have calculated the quantities

$$R_{pn}(k_{\mathrm{rel}}) = \frac{n_A^{pn}}{n_A^{p}} \equiv \frac{pn}{p},$$
$$R_{pp}(k_{\mathrm{rel}}) = \frac{n_A^{pp}}{n_A^{p}} \equiv \frac{pp}{p}, \tag{31}$$
$$R_{pp/pn}(k_{\mathrm{rel}}) = \frac{n_A^{pp}}{n_A^{pn}} \equiv \frac{pp}{pn},$$

where $n_A^{pn} \equiv n_A^{pn}(k_{\mathrm{rel}}, K_{\mathrm{c.m.}} = 0)/n_{\mathrm{c.m.}}^{pn}(K_{\mathrm{c.m.}} = 0)$ and $n_A^{pp} \equiv n_A^{pp}(k_{\mathrm{rel}}, K_{\mathrm{c.m.}} = 0)/n_{\mathrm{c.m.}}^{pp}(K_{\mathrm{c.m.}} = 0)$. Here $n_A^{N_1N_2}$ is related to the process $A(e,e'N_1N_2)X$ and n_A^{p} to the process $A(e,e'p)X$, which includes the contributions from pn and pp SRCs according to Eq. (19), therefore the ratios pn/p and pp/p represent essentially the percentage ratios of the SRCd pp and pn pairs with respect to the total number of SRCd pairs. The quantities in Eq. (31) have been compared with the experimental data by assuming that $p_m \simeq k_{\mathrm{rel}}$, a procedure that implies the validity of the PWIA or, at least, the cancellation of the FSI in the ratios. The comparison is presented in Table IV

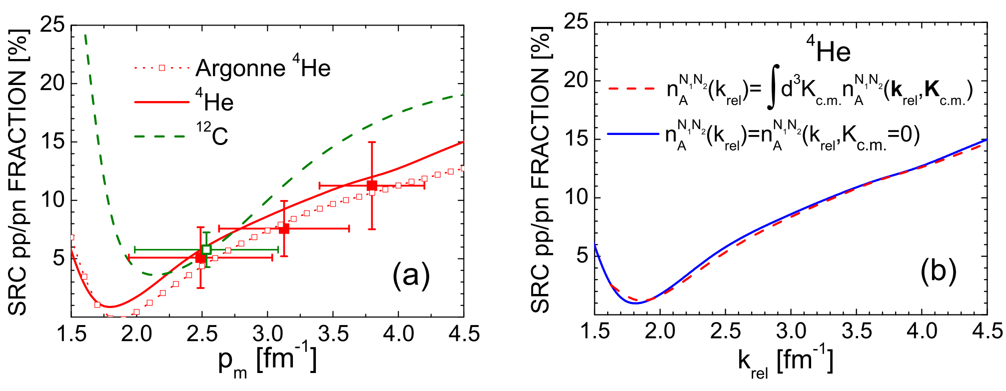

FIG. 15. (a) The experimental percentage of the pN BB pair fraction pp/pn vs the missing momentum p_m, extracted from the processes $^{4}\mathrm{He}(e,e'pn)X$ [30] and $^{12}\mathrm{C}(e,e'pp)X$ [28,29] compared with the quantity $R_{pp/pn}(k_{\mathrm{rel}},0) = n_{pp}(k_{\mathrm{rel}}, K_{\mathrm{c.m.}} = 0)/n_{pn}(k_{\mathrm{rel}}, K_{\mathrm{c.m.}} = 0)$ calculated in the present paper (solid line). Open squares show the results obtained with the Argonne momentum distributions [11]. (b) The same ratio as in (a), calculated within two approaches: (i) solid line, $n_{A=4}^{pp}(k_{\mathrm{rel}}, K_{\mathrm{c.m.}} = 0)/n_{A=4}^{pn}(k_{\mathrm{rel}}, K_{\mathrm{c.m.}} = 0)$; (ii) dashed line, $\frac{\int_0^\infty n_{pp}(k_{\mathrm{rel}}, K_{\mathrm{c.m.}}) K_{\mathrm{c.m.}}^2\, d\, K_{\mathrm{c.m.}}}{\int_0^\infty n_{pn}(k_{\mathrm{rel}}, K_{\mathrm{c.m.}}) K_{\mathrm{c.m.}}^2\, d\, K_{\mathrm{c.m.}}}$.

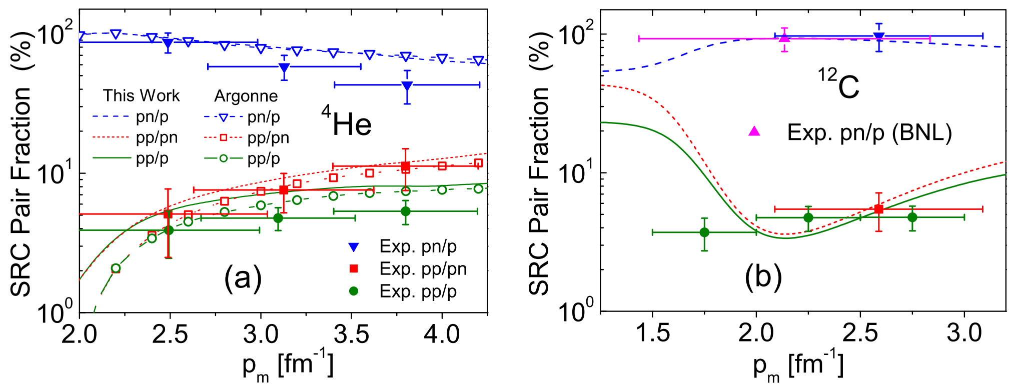

FIG. 16. Experimental percentage of SRC fractions in ^{4}He (a) and ^{12}C (b) compared with theoretical ratios of momentum distributions within the assumption $\mathbf{p}_m \simeq \mathbf{k}_{\rm rel}$ and $K_{\rm c.m.} = 0$. Momentum distributions from the present work and from the Argonne VMC calculation [11]. All experimental data are from Jlab [27–31], except the one represented by the magenta point for ^{12}C, which was obtained from the BNL [26]. In (b) the three theoretical curves were obtained in the present work and correspond to pp/p (solid line), pn/p (dashed line), and pp/pn (dotted line), respectively.

and in Figs. 15 and 16. General agreement between theoretical and experimental percentage ratios appears to hold. Since the experiments have been performed in a momentum region where factorization of the wave functions is at work, the effects of the c.m. motion largely cancel out in the ratios. As for the effects of the FSI the experimental kinematics setup is compatible with the assumption of FSI effects confined within the correlated pair, leading also in this case to some kind of cancellation in the ratio (see, e.g., [2,5,19–22]). Concerning the results presented in these figures the following comments are in order:

(1) Our results for ^{4}He do not practically differ from the ones obtained with the Argonne distributions.
(2) In ^{4}He the increase with $p_m = |\mathbf{p}_m|$ in the pp/pn ratio can be explained by the increasing role of the repulsive NN interaction with respect to the tensor one [Fig. 2(c)]. However, in spite of this satisfactory agreement, an advanced theoretical approach including the FSI is desirable; preliminary results from Refs. [21,22], quoted in Ref. [30], seem to correct the PWIA in the right direction.
(3) The results presented in Fig. 15(b) show that the ratio calculated at $K_{\rm c.m.} = 0$ or integrated by averaging over all directions of $\mathbf{K}_{\rm c.m.}$ practically do not differ, which is another manifestation of factorization since the pp and pn c.m. momentum distributions are essentially the same.

[10]We are grateful to Or Hen for clarifying discussions on these experimental data.

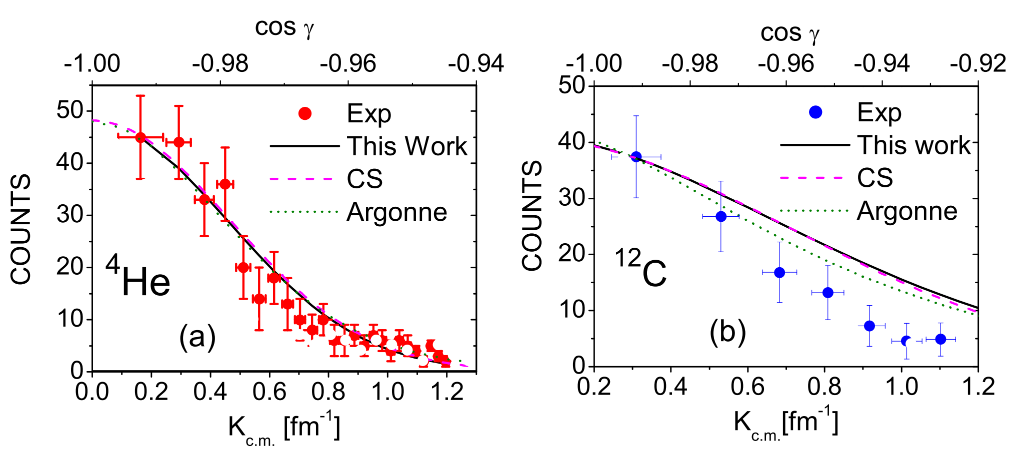

FIG. 17. The c.m. momentum distribution of a pn pair in ^{4}He (a) and a pp pair in ^{12}C (b) obtained in Refs. [30] and [28] from the processes ^{4}He$(e,e'pn)X$ and ^{12}C$(e,e'pp)X$. γ is the angle between $\mathbf{p}_m$ and $\mathbf{p}_{\rm rec}$, which in the PWIA is the angle between $\mathbf{k}_1$ and $\mathbf{k}_2$. The values of $\mathbf{K}_{\rm c.m.}$ have been obtained assuming $\mathbf{k}_2 = -\mathbf{k}_1$. The theoretical curves correspond to the momentum distributions in Ref. [11] (Argonne) and Ref. [25] (CS). Experimental data are given in arbitrary units and theoretical calculations were normalized at the lowest available experimental point. Note that the discrepancy or the agreement between the experimental data and the theoretical calculations might not be real ones, since the latter, unlike the former, do not take into account the finite acceptance and resolution of the detectors and the continuous background. Indeed, when these are taken into account by a proper simulation [28,30,41], the data can be explained by the Gaussian distribution $n_{\rm c.m.}(K_{\rm c.m.}) = (\alpha/\pi)^{1.5}\exp(-\alpha K_{\rm c.m.}^2)$ in agreement with the three curves in (a) and (b).[10]

B. The c.m. momentum distribution of correlated pairs in ^{4}He and ^{12}C

The c.m. momentum distributions of a correlated *pn* pair relative to the spectator nucleus $A-2$ in ^{4}He and the *pp* pair in ^{12}C has been determined in Refs. [28,30] by analyzing the distribution of events in the process $A(e,e'pN)X$ as a function of the cosine of the opening angle γ between $\mathbf{p}_m$ and $\mathbf{p}_{\rm rec}$, which, in PWIA, is the angle between $\mathbf{k}_1$ and $\mathbf{k}_2$. The results of the analysis of the experimental data, are shown in Fig. 17, where the theoretical momentum distributions are also shown. It turns out that, once the experimental data are analyzed taking into account the finite acceptance of the detectors and the continuous background, they nicely agree with the theoretical momentum distributions.

VII. SUMMARY AND CONCLUSIONS

In this paper we have investigated in-medium short-range nucleon-nucleon dynamics by calculating various kinds of two-nucleon momentum distributions in few-nucleon systems and selected isoscalar nuclei with $A \leqslant 40$. To this end, calculations have been performed within a parameter-free many-body approach which, even if not fully *ab initio*, turned out to be capable of treating high-momentum components in nuclei with $A \geqslant 12$, for which advanced VMC approaches with bare strongly repulsive local interactions are, unfortunately, not yet feasible. The method, based upon a linked cluster expansion of one- and two-nucleon, diagonal and nondiagonal, density matrices, has been previously used to calculate the ground-state energy [15] and the momentum distributions [16,17]. In this paper we have performed a detailed analysis of the two-nucleon momentum distributions $n_A^{N_1N_2}(k_{\rm rel},K_{\rm c.m.},\Theta)$ at various values of $k_{\rm rel}$, $K_{\rm c.m.}$, and Θ, as well as of the two-nucleon relative, $n_A^{N_1N_2}(k_{\rm rel})$, and center-of-mass, $n_A^{N_1N_2}(k_{\rm c.m.})$, momentum distributions of proton-neutron and proton-proton pairs. The results of our calculations show that a fundamental property of the nuclear wave function at short internucleon separations turns out to be its factorization into the relative and the c.m. coordinates, a property which has been previously theoretically illustrated in the case of nuclear matter [23] and few-nucleon systems [24]. Such a property is a very relevant one, for it fully governs the high-momentum behavior of two-nucleon momentum distributions generated by short-range correlations. In particular, the following properties of in-medium two-nucleon dynamics, resulting from wave-function factorization, are worth stressing:

(1) In the region of relative distances $r_{ij} \gtrsim 1$–1.5 fm^{-1}, nucleons *i* and *j* move independently in a mean field, with average relative momentum $k_{\rm rel} \lesssim 1.5$–2.0 fm^{-1}, without any particular difference between *pp* and *pn* distributions, apart from those due to the Coulomb interaction; however, as soon as the relative distance decreases down to a value of $r_{ij} \lesssim 1$–1.5 fm^{-1}, the two nucleons start feeling the details of the NN interaction, in particular, the tensor force which causes the *pn* and *pp* motions to differ appreciably, with the difference decreasing at shorter distances, where the strong NN repulsive part of the local NN interaction dominates. In the SRC regions, characterized by a large content of high-momentum components, thanks to the decoupling of the c.m. and the relative motions, also the two-nucleon momentum distribution, independently of the mass of the nucleus, factorizes into a relative and a c.m. part; in particular, in the case of *pn* pairs one has $n_A^{pn}(k_{\rm rel},K_{\rm c.m.},\Theta) \simeq C_A^{pn} n_D^{pn}(k_{\rm rel}) n_{\rm c.m.}^{pn}(K_{\rm c.m.})$, where C_A^{pn} is an A-dependent constant, the *nuclear contact*, which counts the number of deuteron-like pairs in nucleus A, and $n_D(k_{\rm rel})$ is the deuteron momentum distribution. We have shown that the deuteron-like factorized form is valid only at low values of the c.m. momentum, $K_{\rm c.m.} \lesssim 1$–1.5 fm^{-1} and, at the same time, at high values of the relative pair momentum $k_{\rm rel} > k_{\rm rel}^- \simeq 2$ fm^{-1}, with the value of $k_{\rm rel}^-$ increasing with the value of $K_{\rm c.m}$.; thus, the dynamics of in-medium *pn* pairs can, to a large extent, be described as the dynamics of the motion in the nucleus of a deuteron-like pair, whose c.m. moves with a momentum distribution $n_{\rm c.m}^{pn}(K_{\rm c.m.})$.

(2) Within the above picture, arising from the factorization property of the momentum distributions, the ratio $n_A^{pn}(k_{\rm rel},K_{\rm c.m.}=0)/[n_D(k_{\rm rel})n_{\rm c.m.}^{pn}(K_{\rm c.m.}=0)]$ at high relative values of $k_{\rm rel}$ should become a constant equal to C_A^{pn}, which is indeed the case; thus the theoretical values of the contacts C_A^{pn}, which have been determined by plotting the ratio vs $k_{\rm rel}$, are completely free of any adjustable phenomenological parameter, for they are entirely defined in terms of many-body quantities that are fixed by the choice of the NN interaction and by the way the many-body problem is solved. This is true for all nuclei considered, within both our cluster expansion approach and the VMC *ab initio* calculation. The values of C_A^{pn} range from about 2 in ^{3}He to about 60 in ^{40}Ca; for ^{4}He the value of C_A^{pn} is less by about 20% than the value obtained with the VMC momentum distribution; such a difference should be ascribed both to the different Hamiltonian (V8$'$ NN interaction in our case and AV18 in Ref. [11]) and to the different variational wave functions; this point is under quantitative investigation.

(3) For all nuclei that have been considered we found that when $k_{\rm rel} \gtrsim 2$ fm^{-1}, the ratio $n_A^{pn}(k_{\rm rel},K_{\rm c.m.}=0)/[C_A^{pn} n_{\rm c.m.}^{pn}(K_{\rm c.m.})]$ practically does not differ from the deuteron momentum distribution $n_D(k_{\rm rel})$, which is further clear evidence of factorization of $n_A^{pn}(k_{\rm rel},K_{\rm c.m.},\Theta)$. Factorization also occurs when the numerator of the ratio is replaced by the $K_{\rm c.m.}$-integrated momentum distribution $n_A^{pn}(k_{\rm rel})$, obtaining the ratio $n_A^{pn}(k_{\rm rel})/[C_A^{pn} n_{\rm c.m.}^{pn}(K_{\rm c.m.})]$. This, however. is only true at very high values of $k_{\rm rel} \gtrsim 4$ fm^{-1}; this means that at $k_{\rm rel} \gtrsim 4$ fm^{-1}, $n_A^{pn}(k_{\rm rel})$ is dominated by the deuteron-like components with $K_{\rm c.m.}=0$, whereas at lower values of $K_{\rm c.m.}$, also the c.m. components with $K_{\rm c.m.} \neq 0$ contribute.

(4) We have considered the relationships between the one-nucleon and the two-nucleon momentum distribution, a topic recently discussed in Ref. [39]. To this end we have compared three approaches, namely, (i) the

one in which only back-to-back ($K_{\text{c.m.}} = 0$) correlated nucleons are considered; (ii) the convolution model developed in Ref. [25]; and (iii) the approach in Ref. [39], where the two-nucleon momentum distributions are considered in the asymptotic limit $k_1 \gg K_{\text{c.m.}}$. Our results demonstrate that in all three approaches the one-nucleon momentum distribution can be expressed, to a large extent, in terms of a proper sum of the *pn* and *pp* distributions, starting from a value of the one-nucleon momentum $k_1 \gtrsim 2\ \text{fm}^{-1}$, within approaches (i) and (ii) and starting at $k_1 \gtrsim 4\ \text{fm}^{-1}$, within approach (iii).

(5) The two-nucleon momentum distributions have been used to calculate the absolute values of the number of SRCd *pn* and *pp* pairs in the considered nuclei; in particular, we have calculated the number of BB SRCd pairs, defined by the integral of the two-nucleon momentum distribution in correspondence with $K_{\text{c.m.}} = 0$ and (similarly to the deuteron case) in the relative momentum range $1.5 < k_{\text{rel}} < \infty\ \text{fm}^{-1}$, finding in complex nuclei a number of BB SRCd *pn* pairs larger than the number of *pp* pairs by about a factor of 10. Concerning the numbers of SRCd *nucleons* it should be stressed that in our approach the one- and two-nucleon momentum distributions satisfy the exact relationship provided by Eq. (19), which is valid in the entire region of momentum $0 < k_1 < \infty\ \text{fm}^{-1}$, so that the obtained two-nucleon momentum distributions provide a percentage ratio of SRCd nucleons to the total number of nucleons in the range of 16%–20%, if SRCs are defined with respect to a pure independent-particle shell-model description.

(6) The dependence upon k_{rel} and $K_{\text{c.m.}}$ of the two-nucleon momentum distributions of ^{4}He and ^{12}C in the region of SRCs is in good agreement with available experimental data [26–31], and so are the c.m. distributions.

Several aspects of the above picture, which we have shown to occur also in light nuclei ($A \leqslant 12$) treated within the VMC approach [11], have already been experimentally confirmed, whereas some others, concerning, in particular, the values of the nuclear contact in various spin-isospin states, deserve further theoretical and experimental investigations. Finally, we would like to stress that our approach provides momentum distributions that in some momentum regions are lower by 15%–20% than the ones calculated with the VMC momentum distributions; as already pointed out, this can be attributed partly to the different Hamiltonian used in the two approaches and partly to the different variational wave functions; this point is under investigation. To conclude, our approach turned out to be accurate enough to describe the main features of SRCs in few-nucleon systems and isoscalar nuclei with $A \leqslant 40$, so that it should deserve extension to different types of NN interaction models differing, particularly, in short-range behavior, and should be applied to heavier neutron-rich nuclei, whose investigation presents several interesting aspects [31,43].

ACKNOWLEDGMENTS

This work was performed within the activity and support of the Italian Istituto Nazionale di Fisica Nucleare (INFN), Sezione Perugia, to whom H.M. is indebted for kind hospitality and support. We gratefully acknowledge Robert Wiringa for providing useful information on the effects of 3N forces on high-momentum components, within the VMC approach. M.A. was supported by grants provided by the Regione Umbria, under POR-FESR Umbria Contract No. 20072013, asse ii, attività a1, azione 5, and by the Dipartimento della Protezione Civile, Italy; he also acknowledges the CINECA award under ISCRA initiative for making high-performance computing resources available.

[1] L. Frankfurt, M. Sargsian, and M. Strikman, Int. J. Mod. Phys. A **23**, 2991 (2008).
[2] J. Arrington, D. W. Higinbotham, G. Rosner, and M. Sargsian, Prog. Part. Nucl. Phys. **67**, 898 (2012).
[3] M. Alvioli, C. Ciofi degli Atti, L. P. Kaptari, C. B. Mezzetti, and H. Morita, Int. J. Mod. Phys. E **22**, 1330021 (2013).
[4] C. Ciofi degli Atti, in *NN and 3N Interactions* (Nova Science, New York, 2014).
[5] C. Ciofi degli Atti, Phys. Rep. **590**, 1 (2015).
[6] Y. Suzuki and W. Horiuchi, Nucl. Phys. A **818**, 188 (2009).
[7] H. Feldmeier, W. Horiuchi, T. Neff, and Y. Suzuki, Phys. Rev. C **84**, 054003 (2011);
[8] R. Roth, T. Neff, and H. Feldmeier, Prog. Part. Nucl. Phys. **65**, 50 (2010).
[9] R. Schiavilla, R. B. Wiringa, S. C. Pieper, and J. Carlson, Phys. Rev. Lett. **98**, 132501 (2007).
[10] M. Alvioli, C. Ciofi degli Atti, L. P. Kaptari, C. B. Mezzetti, H. Morita, and S. Scopetta, Phys. Rev. C **85**, 021001 (2012).
[11] R. B. Wiringa, R. Schiavilla, S. C. Pieper, and J. Carlson, Phys. Rev. C **89**, 024305 (2014).
[12] M. Gaudin, J. Gillespie, and G. Ripka, Nucl. Phys. A **176**, 237 (1971).
[13] O. Bohigas and S. Stringari, Phys. Lett. B **95**, 9 (1980).
[14] F. Arias de Saavedra, C. Bisconti, G. Co', and A. Fabrocini, Phys. Rep. **450**, 1 (2007).
[15] M. Alvioli, C. Ciofi degli Atti, and H. Morita, Phys. Rev. C **72**, 054310 (2005).
[16] M. Alvioli, C. Ciofi degli Atti, and H. Morita, Phys. Rev. Lett. **100**, 162503 (2008).
[17] M. Alvioli, C. Ciofi degli Atti, L. P. Kaptari, C. B. Mezzetti, and H. Morita, Phys. Rev. C **87**, 034603 (2013).
[18] L. L. Frankfurt and M. I. Strikman, Phys. Rep. **160**, 235 (1988).
[19] L. L. Frankfurt, M. M. Sargsian, and M. I. Strikman, Phys. Rev. C **56**, 1124 (1997).
[20] I. Mardor, Y. Mardor, E. Piasetsky, J. Alster, and M. M. Sargsyan, Phys. Rev. C **46**, 761 (1992); C. Ciofi degli Atti and L. P. Kaptari, Phys. Rev. Lett. **100**, 122301 (2008).
[21] J. Ryckebusch, D. Debruyne, P. Lava, S. Janssen, B. Van Overmeire, and T. Van Cauteren, Nucl. Phys. A **728**, 226 (2003).
[22] W. Cosyn, M. C. Martinez, and J. Ryckebusch, Phys. Rev. C **77**, 034602 (2008).

[23] M. Baldo, M. Borromeo, and C. Ciofi degli Atti, Nucl. Phys. A **604**, 429 (1996).
[24] C. Ciofi degli Atti, L. P. Kaptari, S. Scopetta, and H. Morita, Few Body Syst. **50**, 243 (2011).
[25] C. Ciofi degli Atti and S. Simula, Phys. Rev. C **53**, 1689 (1996).
[26] A. Tang, J. W. Watson, J. Aclander, J. Alster, G. Asryan, Y. Averichev, D. Barton, V. Baturin, N. Bukhtoyarova, A. Carroll, S. Gushue, S. Heppelmann, A. Leksanov, Y. Makdisi, A. Malki, E. Minina, I. Navon, H. Nicholson, A. Ogawa, Y. Panebratsev, E. Piasetzky, A. Schetkovsky, S. Shimanskiy, and D. Zhalov, Phys. Rev. Lett. **90**, 042301 (2003).
[27] E. Piasetzky, M. Sargsian, L. Frankfurt, M. Strikman, and J. W. Watson, Phys. Rev. Lett. **97**, 162504 (2006).
[28] R. Shneor *et al.* (Jefferson Lab Hall Collaboration), Phys. Rev. Lett. **99**, 072501 (2007).
[29] R. Subedi *et al.*, Science **320**, 1476 (2008).
[30] I. Korover *et al.* (Lab Hall Collaboration), Phys. Rev. Lett. **113**, 022501 (2014).
[31] O. Hen *et al.*, Science **346**, 614 (2014).
[32] A. Kievsky, S. Rosati, and M. Viviani, Nucl. Phys. A **551**, 241 (1993).
[33] A. Kievsky, M. Viviani, L. Girlanda, and L. E. Marcucci, Phys. Rev. C **81**, 044003 (2010).
[34] H. Morita (unpublished).
[35] R. B. Wiringa, V. G. J. Stoks, and R. Schiavilla, Phys. Rev. C **51**, 38 (1995).
[36] B. S. Pudliner, V. R. Pandharipande, J. Carlson, S. C. Pieper, and R. B. Wiringa, Phys. Rev. C **56**, 1720 (1997).
[37] R. B. Wiringa, Private communication.
[38] S. Tan, Ann. Phys. **323**, 2952 (2008).
[39] R. Weiss, B. Bazak, and N. Barnea, Phys. Rev. C **92**, 054311 (2015).
[40] O. Hen, L. B. Weinstein, E. Piasetzky, G. A. Miller, M. M. Sargsian, and Y. Sagi, Phys. Rev. C **92**, 045205 (2015).
[41] O. Hen and E. Piasetzky, Private communication.
[42] R. Schiavilla, V. R. Pandharipande, and R. B. Wiringa, Nucl. Phys. A **449**, 219 (1986).
[43] M. M. Sargsian, Phys. Rev. C **89**, 034305 (2014).